REVIEW

ADVANCED
ELECTRONIC
MATERIALS
Open Access

www.advelectronicmat.de

Equilibrium or Non-Equilibrium – Implications for the Performance of Organic Solar Cells

Dorothea Scheunemann, Clemens Göhler, Constantin Tormann, Koen Vandewal, and Martijn Kemerink*

With power conversion efficiencies approaching 20%, organic solar cells can no longer be considered the ugly duckling of photovoltaics. Successes notwithstanding, there is still a need for further improvement of organic solar cells, both regarding energy and current management in these devices. At present, there are different and mutually exclusive interpretation schemes for the associated losses of energy and charge, hampering the rational design of next generations of organic solar cells. One critical factor that affects voltage, current, and fill factor losses is whether or not photogenerated charges are effectively near or far away from thermodynamic equilibrium. While it is commonly agreed that both the vibronic and (disordered) energetic structure of organic semiconductors affect the solar cell characteristics, the degree to which deviations from near-equilibrium population of the associated energy level distributions matter for the photovoltaic performance is unclear: near-equilibrium as well as kinetic descriptions have provided seemingly convincing descriptions of a wide range of experiments. Here, the most important concepts in relation to experimental results are reviewed, open questions are addressed and implications for device performance and improvement are highlighted.

1. Introduction

Nowadays, efficiencies of organic solar cells approach those of competing solar cell technologies, making the organics less of an outlier in the photovoltaic (PV) family. The same appears to hold for the conceptual understanding that guides most of today's optimization strategies of organic PV (OPV). While these strategies have proven to be very successful, there is good reason to reconsider some of the, usually tacit, assumptions about the internal workings of OPV devices that underlie them. With this review, we hope to make the reader aware that this is not only an academic affair but might well lead to so far unexplored approaches and design rules to further improve next generations of organic solar cells (OSC).

A simple, phenomenological comparison with state-of-the-art inorganic systems quickly reveals that OPV suffers from disproportionate energy losses, measured as the difference between the energy of the absorbed photons and the open circuit voltage, and, to a lesser degree, to fill factor losses, measured as a reduced squareness of the current-voltage (JV) curve under illumination.[1] Especially the former, voltage losses, are understood as consisting of three dominant factors, which all relate to peculiarities of the commonly used organic semiconductor blends of donor and acceptor materials.[2] First, the low dielectric constant and the large overlap between the highest occupied molecular orbital (HOMO) and lowest unoccupied molecular orbital (LUMO) wavefunctions lead to exciton binding energies that much exceed the thermal energy and necessitate the use of donor-acceptor blends in which an appropriate energy level offset drives the transfer of one of the constituent charges of the exciton that sits on material A to the other material B, splitting the exciton.[3] Second, photovoltaic blends typically make very poor light emitters, whose external quantum efficiency of electroluminescence (EQE_{EL}) can be directly linked to voltage losses via thermodynamic considerations.[4] Third, energetic disorder leads to tails of localized states inside the bandgap, in which photogenerated charges can thermalize.[5]

The similarity in conceptual understanding of organic and inorganic PV systems does not sit in these factors by themselves, but in the fact that they are analyzed and interpreted using models that critically rely on the notion that OPV devices can be considered to operate in near-equilibrium conditions. Here, the term "near-equilibrium" can loosely be understood as electron and hole populations each being in equilibrium with the lattice, that is, being characterized by a Fermi-Dirac distribution with a

D. Scheunemann, C. Göhler, C. Tormann, M. Kemerink
Institute for Molecular Systems Engineering and Advanced Materials
Heidelberg University
69120 Heidelberg, Germany
E-mail: martijn.kemerink@cam.uni-heidelberg.de
K. Vandewal
Institute for Materials Research (IMO-IMOMEC)
Hasselt University
Wetenschapspark 1, Diepenbeek 3590, Belgium

characteristic temperature that equals that of the rest of the sample and a quasi-Fermi level $E^{\star}_{F,n/p}$ that differs for electrons (n) and holes (p). In full equilibrium, one would have $E^{\star}_{F,n} = E^{\star}_{F,p}$ and the device would not be able to deliver any power. Near-equilibrium, energy level offsets one-on-one translate into energy losses, as does thermalization in the disorder-broadened density of states (DOS); under these conditions, a sub-unity EQE_{EL} translates to a loss in open circuit voltage V_{OC} of $q\Delta V_{OC} = k_B T\ln(EQE_{EL})$ with q the elementary charge and k_B Boltzmann's constant as discussed in detail below. In turn, these factors rationalize the currently popular mitigation strategies of driving force reduction and suppression of nonradiative recombination and disorder.[6] The Theory and Observables sections below will discuss the near-equilibrium thermodynamic model along with some of its most successful applications to experiments, as well as some of its shortcomings.

Despite the predictive and guiding qualities of near-equilibrium models, there are experimental and theoretical results that cast doubt on the validity of the near-equilibrium assumption. Stepping ahead of the more detailed discussions in the following sections, there are at least two well-established time windows in the event chain from photon absorption to charge extraction at which photogenerated charges may not at all be in near-equilibrium: at very short (∼ps) time scales after absorption (and possibly after charge transfer), the photogenerated charges will likely populate states that are vibronically hot. Such states might be more delocalized and give rise to coherent or band-like motion that is no longer observed once the charge has (locally) cooled down. At long (∼μs) time scales, charges thermalize in the broadened DOS, which is a slow process as sites around typical equilibrium energies are rare, and charges have to travel over relatively large distances to reach them. During this process, motion is potentially strongly diffusive and characterized by an enhanced (transient) mobility, driven by the ongoing energy loss. Note that also charge carrier lifetimes in operational OPV devices under solar irradiation are in the μs range,[7] and even longer at low intensities.[7]

Before turning to a more detailed description of processes in OPV, it is interesting to consider the question of to which degree randomizing or diffusive forces might be expected to be important and to which degree non-equilibrium effects might contribute to that. For this purpose, the Péclet number, which is commonly used in fluid dynamics and defined as the ratio of advective over diffusive transport rates, is useful. Applied to a photogenerated charge that responds to deterministic and diffusive forces that act on a relevant characteristic length scale, it can be written as

$$Pe = \frac{E^{\text{typ}}_{\text{drift}}}{E^{\text{typ}}_{\text{diff}}} \tag{1}$$

where we have expressed Pe in terms of characteristic energies instead of forces by multiplying with a typical length scale. The factors $E^{\text{typ}}_{\text{drift}}$ and $E^{\text{typ}}_{\text{diff}}$ are then the energies associated with deterministic and stochastic motion, respectively. We will focus on the effects of energetic disorder, which is characterized by a Gaussian density of localized states of width σ_{DOS} in the order of 0.05–0.1 eV and inter-site transport. Moreover, we will assume

that photogeneration occurs at $t = 0$ on a random site in the DOS, such that thermalization over an energy $\approx \sigma_{\text{DOS}}$ must occur by inter-site motion for near-equilibrium to set in. At short time scales, that is prior to thermalization, Pe then becomes $Pe \approx qa_{\text{NN}}F/\sigma_{\text{DOS}} \approx 10^{-2} \ll 1$ for the nearest neighbor distance $a_{\text{NN}} \approx 1$ nm and an extraction field $F \approx 10^6$ V m^{-1}, implying that inter-site carrier motion will be completely random. At the longer time scales at which extraction occurs, one gets $Pe \approx qLF/k_B T$, where L is the device thickness ≈ 100 nm and $k_B T \approx 0.025$ eV the thermal energy at ambient temperature, giving $Pe \approx 4 > 1$. Hence, at these time scales, directed transport will dominate, provided that $k_B T$ is indeed the relevant energy scale. This, in turn, demands that thermalization in the DOS has completed, implying an energy loss of the order of magnitude of σ_{DOS}. Incomplete thermalization before charge carrier extraction might limit these energy losses, albeit at the price of more diffusive motion. Unless the contacts are perfectly selective, the latter will reduce the photocurrent due to charges ending up at the wrong contact. Summarizing this short digression on the Péclet number, it may be anticipated that transport, i.e., separation and extraction, of photogenerated charges in OPV is significantly more diffusive than expected on basis of the lattice thermal energy alone. It highlights the critical role of the thermalization time in relation to the other relevant time scales in the system, e.g. for recombination and extraction.

1.1. Theory

In its most general form, an organic solar cell consists of an organic absorber layer, sandwiched between two, ideally charge-selective, contacts, as illustrated in Figure 1. An ideal contact is here a contact where there is no energetic barrier to inject or extract one type of carrier, which is the majority type carrier. Extraction or injection of the other type of carrier, the minority carrier, will be heavily suppressed. The absorber layer consists of a blend between an electron donor (often a polymer) and (small molecule) acceptor. In this layer incident (solar) photons are converted efficiently into mobile charge carriers in a rather complex and debated process described below. The free electrons and holes move under the influence of a built-in or external electric field (drift) and diffusion. Charges are extracted at their respective electrode, producing a photocurrent. The directionality of charge extraction might be achieved using contacts with appropriate (different) work functions, or alternatively by using p- or n-type doped interlayers, resulting in hole and electron selectivity, respectively. Both result in an internal electrostatic field which is sufficient to extract most of the photo-generated charges.

Applying a negative voltage over the device increases this field. A positive voltage decreases this electric field and will result in the diffusive injection of electrons and holes at their respective electrode (Figure 1). The high charge density in the device at forward voltages will result in a significant increase in the electron-hole encounter probability and thus in a significant recombination current. At open-circuit, this recombination balances with the photocurrent, setting the open-circuit voltage (V_{OC}). The question whether this balance is thermodynamic, i.e., involving recombination of the equilibrated, photogenerated charges, or kinetic, due to balancing photo- and injection-currents that need not be in thermodynamic equilibrium, is experimentally hard to
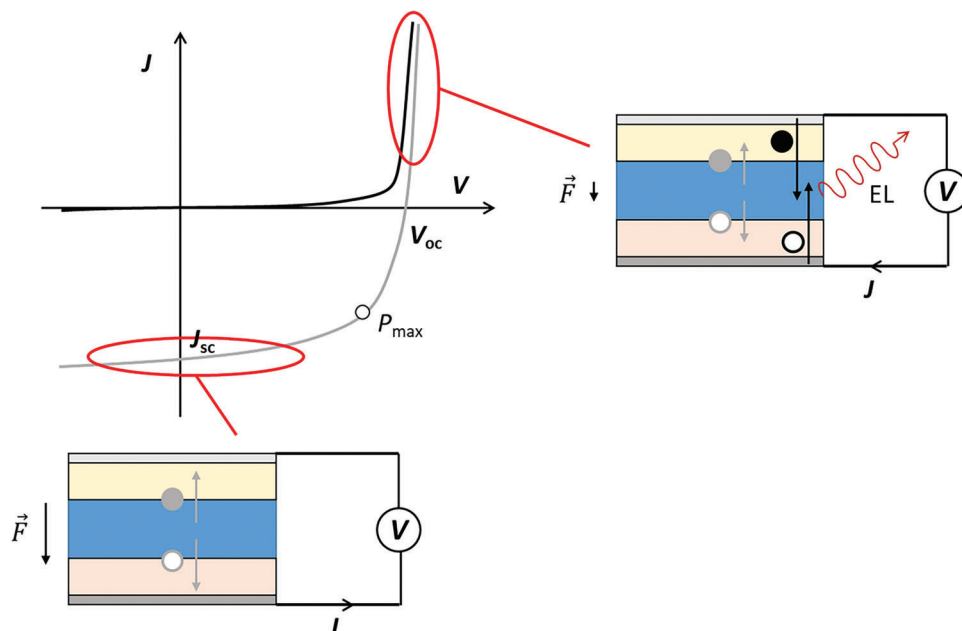
**ADVANCED
SCIENCE NEWS**

www.advancedsciencenews.com

**ADVANCED
ELECTRONIC
MATERIALS**

www.advelectronicmat.de

Figure 1. Current density (J) – voltage (V) curves, in darkness (black) and under illumination (gray). Open-circuit voltage (V_{OC}), short-circuit current (J_{SC}) and the maximum power point (P_{max}) where the absolute value of the $J \cdot V$ product is maximal in the power-generating quadrant is indicated in the graph. At voltages around short-circuit charges are extracted with the aid of an electric field over the active layer, as indicated schematically in the lower part of the figure. At voltages sufficiently high to inject charges, the electric field $\vec{F}$ over the active layer is reduced. Charges are injected via the selective contacts and recombine within the active layer. The recombination event can result in photon emission by electroluminescence (EL), schematically indicated on the right-hand side of the figure.

answer and will be discussed later in this review. At short circuit, the charge density within the photo-active layer is low, as no charges are injected and the electric field is sufficiently high to quickly remove the charge carriers out of the photo-active layer. The electron-hole encounter probability and the recombination current are therefore low and the short-circuit current (J_{SC}) is therefore close or equal to the current produced by the photo-generated charges.

At the working point of the solar cell, the generated power, which is the product of the net-generated current and applied voltage, is maximal. The power conversion efficiency (PCE) is the maximum generated power (P_{max}), divided by the illumination intensity. A high PCE implies that the voltage and current at the maximum power point are close to V_{OC} and J_{SC}, respectively. The ratio between P_{max} and the $V_{OC} \cdot J_{SC}$ product defines the fill factor (FF) of the device, which in the best organic solar cells can be up to 0.8.[8]

In the dark, organic solar cells show the current-voltage characteristic of a diode: when a forward voltage is applied, electrons and holes are injected into the absorber layer. When the contacts are selective, these injected charges can only leave the absorber layers by recombining with an opposite sign charge carrier. The current at forward voltages in such devices is thus entirely a recombination current and can therefore result in an emitted photon-flux; this electroluminescence (EL) becomes brighter when non-radiative pathways are removed. The EL spectrum and quantum efficiency are thus expected to contain information on the recombination pathways within the photo-active layer. The quantitative relation between (non-)radiative recombi-

nation and photovoltaic performance of the OPV device is discussed further in later sections.

Let us now look in more detail at the microscopic charge generation and recombination processes proceeding within the photo-active layer when illuminated. Here, we will follow the arrows in the energy (state) diagram in Figure 2. Photon-absorption results in the creation of a singlet exciton which upon creation has the same energy as the photon. Several excited state
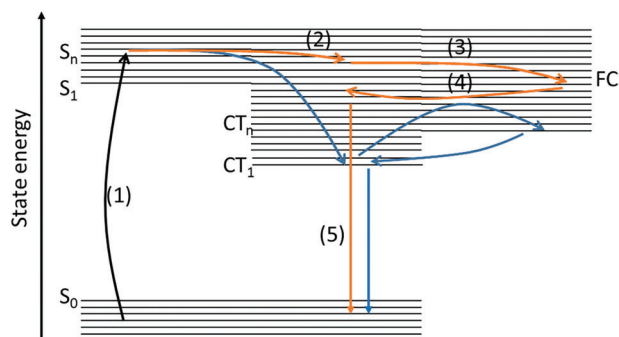

Figure 2. State diagram at the donor-acceptor interface. Optical excitation of the ground-state (S_0) of the donor or acceptor results generally in an electronically and vibrationally excited state S_n. The electronic processes indicated by the arrows (1)–(4) and associated energy losses are discussed in the main text. Blue arrows indicate pathways where equilibration within the CT state occurs before further dissociation. Orange arrows indicate out-of-equilibrium pathways where equilibration within the CT state manifold does not occur before dissociation.

2300293 (3 of 23)

**ADVANCED
SCIENCE NEWS**

www.advancedsciencenews.com

**ADVANCED
ELECTRONIC
MATERIALS**

www.advelectronicmat.de

processes result in the dissipation of this energy. Relaxation within the excited state energy levels is possible, but when the exciton is created in close proximity to the donor-acceptor interface, electron transfer competes with this relaxation process, and charge transfer from higher energy singlet (S_n) states occurs.[9] However, also the relaxed singlet (S_1) dissociates efficiently in the highest-performance OPV blends, as in these devices, the absorbed photon-to-collected-charge conversion yield (or internal quantum efficiency, IQE) upon S_1 excitation is near unity.[10] Charge-transfer (CT) states formed upon dissociation (process (2) in Figure 2) might therefore have some excess energy, which can in principle be dissipated within the CT state manifold. A CT state is hereby defined as the interfacial electronic state, coupled to the ground state, where the electron is on the acceptor and the hole resides on the donor.[11] A CT state can thus decay to the ground state, or further dissociate into separate positive and negative free charge carriers (process (3) in Figure 2). Fast dissociation of higher energy CT states will result in free carriers with (orange arrows in Figure 2) or without (blue arrows in Figure 2) a significant amount of vibronic excess energy. These carriers remain in the photo-active layer, relaxing further, until extracted or until they encounter a charge carrier of opposite sign, forming a CT state (arrow (4) in Figure 2), which then can re-dissociate or recombine (process (5) in Figure 2). In principle, the CT state can also populate an excited triplet state (T_1) in either the donor or the acceptor material, but the relevance of this pathway is debated and, in view of the long triplet lifetimes, likely governed by equilibrium statistics and outside the scope of the present discussion.[12] The debate in the field to be covered here is on which timescales and to what extent the excess energy is dissipated within the steps described above. The extremes of the opposing views encountered in the literature are shown in Figure 2.

The view indicated by the blue arrows is that the free carriers extracted at the electrodes, as well as the recombining CT states, are vibronically fully thermalized. Furthermore, the lowest energy CT state (CT_1) dissociates efficiently and its dissociation yield determines the overall dissociation yield.[13] An alternative view (indicated by the orange arrows) is that free carriers are locally "hot", i.e., vibronically non-thermalized and that recombination occurs from non-thermalized states.[14] As it is the energy and kinetics of the recombining state which determine the photovoltage, both views would result in different design rules for future OPV materials. For OPV following the relaxed pathway, it is conversion of CT_1 to the ground state which should be suppressed, while for devices relaying on the non-thermalized pathway, it is the conversion of CT_n to CT_1 which should be inhibited as much as possible. Similar questions arise when one adds the complications due to energetic disorder, which introduces another, slower, time scale of thermalization and will be discussed in more detail below. Interestingly, the corresponding schematic would be largely identical to Figure 2, but the meaning of the horizontal lines would change from vibronic levels of a single oscillator to ground state energies of a distribution of localized states.

Solving the question through which pathway charges follow requires experimental determination of all involved states and all rate constants at which relaxation and dissociation processes take place. The extent to which there is energetic disorder and via which mechanisms energetic disorder is introduced should
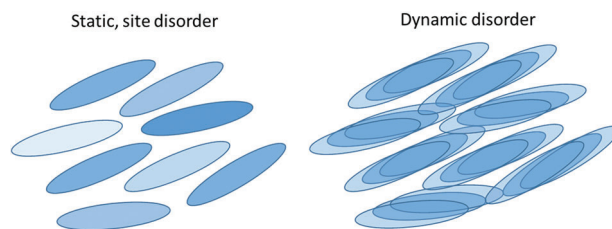

Figure 3. Schematic representation of static and dynamic disorder. The blue ovals indicate chromophores with, in the case of static disorder, the shade of blue being an indication of the average energy of the chromophore. Dynamic disorder results from the vibrations and rotations within the chromophores as well as relative to the neighboring chromophores. The energy at the different sites thus varies in time.

be resolved. Energetic spread on the energy levels of all of these states is the combined result of static and dynamic disorder.[15,16] The difference between these types of disorders is illustrated in Figure 3. Static disorder results in a spread of the energy levels at a certain site due to its specific environment of orientation with the rest of the sites. Dynamic disorder is a consequence of the thermal vibrations of the nuclei within molecular sites or vibration of two molecular sites with respect to each other. When reducing the temperature these vibrational modes are less populated, with at very low temperatures only the zero point oscillations remaining.

Following a charge carrier (population) as it moves through the kinetic diagram in Figure 2, we will briefly discuss the processes it encounters along the way, with an emphasis on potential non-equilibrium effects.

Accounting for the strong electron-phonon coupling in organic semiconductors, the absorption spectrum (process (1) in Figure 2) is commonly written as[2]

$$A(\hbar\omega) \propto [n(\hbar\omega)\,\hbar\omega] \cdot \sum_m \frac{e^{-S} S^m}{m!} \cdot \Gamma\left(\hbar\omega - \left(\hbar\omega_{0-0} + m\hbar\omega_{ph}\right)\right) \quad (2)$$

where S is the Huang-Rhys factor, m is the number of vibrational levels (number of vibronic peaks), and Γ and $\hbar\omega_{0-0}$ are the line shape and the central energy of the 0-0 transition, and $\hbar\omega_{ph}$ is the dominant phonon mode; a more general expression is obtained by summing over multiple phonon modes.[2] In the presence of strong energetic disorder, the line shape reflects a simple convolution of the occupied (HOMO) and unoccupied (LUMO) densities of states, possibly weighted by an (unknown) energy dependence of the matrix element. The reorganization energy λ that appears in the semiclassical Marcus model, c.f. Equation 4 below, relates to the parameters used here as $\lambda = S\hbar\omega_{ph}$.[2,17] As it stands, Equation 2 contains no direct reference to temperature as it has been derived under the assumption that only the lowest vibronic state is occupied. As this condition is also realistic for OPV under practical operational conditions, any non-equilibrium effects on the S_0–S_n absorption spectra of OPV can be assumed to be limited to photo-induced bleaching, which is typically in the 10^{-4}–10^{-3} range and thus irrelevant for performance.[7] Note that Equation 2 applies to both S_0-S_n and S_0-CT absorptions, possibly with different dominant phonon modes.[18]

Equation 2 indicates a significant probability that directly after excitation, the photoexcited electron-hole pair populates a

vibronically excited state. Although the subsequent thermalization to the vibronic ground state is believed to occur on the ps timescale, this leaves a window for ultrafast "hot carrier" effects that might contribute to an efficient charge transfer (process (2) in Figure 2) and/or charge separation (process (3) in Figure 2).[14,19,20] Specifically, Grancini et al. argued that excess photon energy with respect to the optical gap contributes to the charge generation efficiency because it allows for a resonant coupling between the nascent singlet exciton and hot interfacial states, which are more delocalized in nature and thus more prone to ultrafast charge separation instead of relaxation to the bound CT_1 state.[21] Although the original paper has been heavily criticized for not properly accounting for cavity effects, the general idea of delocalized excited states contributing to efficient charge generation is by now commonly accepted.[22–24] In a seminal paper, Gélinas et al. interpreted transient electroabsorption spectra in terms of ultrafast (<40 fs) delocalization of the electron wavefunction into acceptor aggregates.[25] In a preceding paper, the same group used a pump-push experiment to demonstrate an enhanced dissociation probability of bound interfacial CT-states upon absorption of an infrared "push" photon that was argued to promote bound charge pairs to higher-lying, delocalized bandlike states.[26] Theoretical studies have highlighted various aspects of charge carrier delocalization, enhancing the probability of charge carrier separation over distances of up to tens of angstroms.[20,27–29] Note, in this context, that (enhanced) charge carrier delocalization is not limited to vibronically excited states, and may also occur because of the wavefunctions of thermalized states spreading out due to aggregation, conjugation, or simply low tunneling barriers.[30] These factors do share the property that they lead to deeper, more relaxed states becoming more localized than higher-lying ones.[31]

While vibronic "hotness" may contribute to charge transfer and short-range charge separation, it cannot contribute to long-range transport by hopping due to the strong coupling to molecular vibrations and the associated rapid cooling to the vibronic ground state. For such "cold", on-site relaxed charges, the transport is generally described in terms of thermally activated tunneling or hopping between discrete sites that are localized both in real and energy space. The most commonly employed expressions for the hopping rate ν_{if} between an initial site i with energy E_i to a final site j with energy E_j are due to Miller-Abrahams, viz.[2]

$$\nu_{ij} = \begin{cases} \nu_0 \exp\left(-2\alpha r_{ij}\right) \exp\left(-\frac{E_j - E_i}{k_B T}\right), & E_j > E_i \\ \nu_0 \exp\left(-2\alpha r_{ij}\right), & E_j \leq E_i \end{cases} \tag{3}$$

and Marcus, viz.

$$\nu_{ij} = \nu_0 \, \exp\left(-\frac{\left(E_j - E_i + \lambda\right)^2}{4\lambda k_B T}\right) \tag{4}$$

Here, ν_0 is the attempt to hop frequency, α the inverse localization length, r_{ij} the inter-site distance and λ the reorganization energy. Equations 3 and 4 are derived on basis of different assumptions and can lead to different predictions for thermalizing charges in a strongly energy-dependent DOS. For example, the mean hopping distance increases for progressing thermalization for Miller-Abraham rates, but not for Marcus rates. However, for computational reasons, numerical simulations are often conducted on regular lattices with parameters that make hops to non-nearest neighbors very unlikely, irrespective of initial energy. In that limit, Equations 3 and 4 lead to very similar predictions when used to model charge transport in strongly disordered systems.[32] Specifically, the slow thermalization of charges that will be discussed below, occurs irrespective of the hopping rate expression used.

The site energies E_i are generally believed to be randomly distributed according to a strongly energy-dependent DOS, typically of exponential or Gaussian shape. In both cases, the thermalization of charges toward some equilibrium energy follows a log-linear time dependence, that is, thermalization slows down dramatically with time, see Figure 4.[33,34] The physical reason for the slowdown is that deeper sites become increasingly rare, and therefore partially relaxed charges have to first be re-activated toward transport energy before they can find a deeper lying site. At longer times, the thermalization will saturate at either the Fermi energy, for exponential DOS and Gaussian DOS beyond the Boltzmann limit, or at the equilibrium energy $E_\infty = -\sigma_{\text{DOS}}^2 / k_B T$ for Gaussian DOS in the Boltzmann limit.

Since charge extraction in state-of-the-art OPV devices is rather efficient, the charge carrier densities in such devices are generally low; for 1 Sun conditions, typical values are $\approx 10^{22}$ m^{-3}, which translates into a concentration of 10^{-5} for a number density of 10^{27} m^{-3} for $a_{\text{NN}} = 1$ nm.[7] Concomitantly the electron and hole quasi-Fermi levels lie deep in the tail of their respective DOS. This, in turn, will enhance the relaxation time, i.e., the time needed for thermalization. A rough estimate can be made on basis of the results from Pautmeier et al., see also Figure 4b.[35] Using kinetic Monte Carlo simulations, they found that the relaxation time t_{rel} follows the empirical relation

$$\frac{t_{\text{rel}}}{t_0} = 10 \cdot \exp\left(-\left(1.07 \cdot \hat{\sigma}\right)^2\right) \tag{5}$$

with $t_0 = (6\nu_0 \exp(-2\alpha a_{NN}))^{-1}$ the dwell time, and $\hat{\sigma} = \sigma_{\text{DOS}} / k_B T$ the normalized Gaussian disorder. Assuming a very modest Gaussian disorder of $\hat{\sigma} = 2$ and further $2\alpha a_{NN} = 10$ and $\nu_0 = 10^{11}$ s^{-1}, one has $t_0 \approx 4 \cdot 10^{-8}$ s and $t_{rel} \approx 40$ μs. Since the charge carrier lifetime in OPV around open circuit conditions is below 10 μs, one cannot upfront assume thermalization to complete prior to extraction or recombination.[7]

It was discussed in the context of Equation 1 above that the thermalization of photogenerated charges in the DOS constitutes an energy loss, which may be as large as several hundreds of meV.[5,36] At the same time, the excess energy in the distribution of localized but "vibronically cold" states constitutes an energy reservoir that may be used to overcome any remaining Coulomb binding energies and that leads to transient higher-than-equilibrium mobility.[34,37–39] The physical reason for the latter is the larger density of final sites to hop to that lie at comparable or lower energy than the initial site when the latter is less relaxed in the DOS. According to Equations 3 and 4, this gives rise to higher-than-equilibrium hopping rates and thereby a higher (transient) mobility as illustrated in Figure 5.

It is important that the use of the hopping rates Equations 3 or 4 in kinetic models for OPV devices assures that the charge
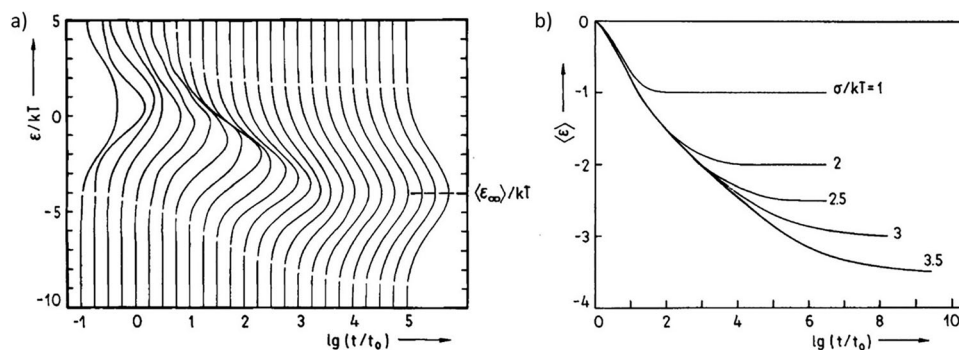
Figure 4. a) Temporal evolution of the charge carrier energy distribution in a Gaussian DOS of width $\sigma_{DOS} = 2k_BT$. ϵ_∞ denotes the theoretical mean energy in the long-time limit. b) Time decay of the mean energy of an ensemble of charge carriers moving within a Gaussian DOS of width $\hat{\sigma} = \sigma_{DOS}/k_BT$. Reproduced with permission.[34] Copyright 1993 Wiley.

transport obeys detailed balance at the microscopic level, which should be the case when it is assumed that charges are "locally cold", i.e., have relaxed to the local ground state. This does not imply that the macroscopic system obeys detailed balance under operating conditions. In fact, the results in Figures 4 and 5 above suggest that charges that have been optically generated at random energy in the DOS will travel to the electrodes using another ("hot") subset of states than the "cold" charges that travel from the electrodes (thermal reservoirs) to recombine in the bulk of the device. In such systems, reciprocity between photovoltaic quantum efficiency (charges out per photons in) and electroluminescence (photons out per charge in) may be broken.[40]

The higher hopping rates for less thermalized charges may also be expected to affect the recombination of photogenerated charges (process (5) in Figure 2). On the one hand, kinetic Monte Carlo simulations of recombination of equilibrated charges in 3D isotropic media indicated recombination rates that are close to the equilibrium Langevin value, with deviations arising due to geometric constraints, anisotropy, and mobility imbalances.[41,42] On the other hand, under the non-equilibrium conditions that

arise when photogenerated charges are still thermalizing, hopping rates may exceed the recombination rate by orders of magnitude, leading to a high probability of (re-)dissociation of electron-hole pairs in a CT or exciton state, in turn leading to actual recombination rates that are orders of magnitude lower than the Langevin value.[43–45]

For electron-hole pairs for which the association into a CT or exciton leads to actual recombination, the electroluminescence spectrum has the reciprocal form to Equation 2, viz.[2]

$$\phi_{EL}(\hbar\omega) \propto [n(\hbar\omega)\hbar\omega]^3 \cdot \sum_m \frac{e^{-S}S^m}{m!} \cdot \Gamma\left(\hbar\omega - (\hbar\omega_{0-0} - m\hbar\omega_{ph})\right) \quad (6)$$

Note, however, that even in the case that thermalized charges recombine, as is the case in a low-bias electroluminescence experiment, the line shape $\Gamma(E)$ may deviate from what would naively be expected, i.e., from a simple convolution of (thermalized occupations of) the HOMO and LUMO densities of states. This happens due to the fact that at least one of the recombining charges
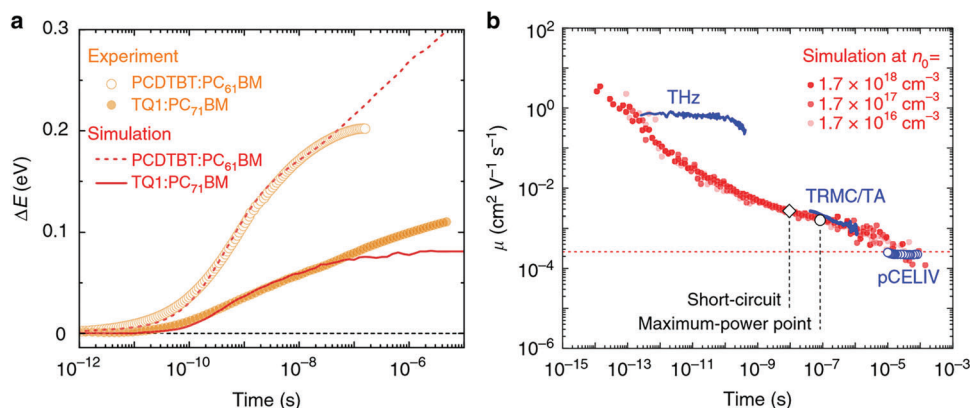

Figure 5. Hole thermalization and the corresponding transient mobility. a) Measured hole relaxation in a TQ1:PC71BM blend (filled orange circles) and a PCDTBT:PC61BM blend (empty orange circles) and the results from kMC simulations (dashed and solid red lines). The center of the hole DOS (HOMO level) sits at the black dashed line. b) Measured time-dependent mean mobility of a TQ1:PC71BM blend from various experiments, indicated in the figure (blue lines and symbols), and kMC simulations at the indicated initial carrier densities n_0 (red symbols). The red dashed line indicates the equilibrium mobility corresponding to the simulation parameters. The black empty diamonds and black empty circles indicate the extraction time at short-circuit and at maximum-power point respectively, highlighting the incomplete thermalization under operational conditions. Reproduced under the terms of the CC BY license.[36] Copyright 2015, the authors, published by Springer Nature.

**ADVANCED
SCIENCE NEWS**

www.advancedsciencenews.com

**ADVANCED
ELECTRONIC
MATERIALS**

www.advelectronicmat.de

has to be excited toward transport energy in order to reach its recombination partner.[18,46]

2. Observables

In this section, we address a range of directly measurable quantities, including some key performance indicators of OPV devices. Although the interpretation of these observables may vary between different authors, which is the topic of this review, the quantities themselves can directly be extracted from experiments and do not require an interpretation step.

2.1. Electro- and Photoluminescence

A straightforward experimental method to investigate the energetic distribution of charge carriers in the DOS is the spectral analysis of their recombination energy from luminescence (non-thermal emission of radiation). For OSCs, relevant cold emission is induced by applying a photochemical or electrochemical potential to study either photo- (PL) or electroluminescence (EL).[13,15,16,47–54] In general, luminescence experiments usually result in one or more of three basic observables: the spectral distribution of emitted radiation given by the flux $\phi_L(\hbar\omega)$, the radiative recombination efficiency EQE_L, and the temporal evolution in the form of emission transients. The emitted photon flux ϕ_L can, in accordance with Kasha's rule[55] and Würfel's generalization of Kirchhoff's law,[56] be expressed by the grey body emission $(A(\hbar\omega)\phi_{BB}(\hbar\omega, T))$ amplified by the applied chemical potential μ:

$$\phi_L(\hbar\omega)\, d\omega = \sum_i \eta_i A_i(\hbar\omega)\, \phi_{BB}(\hbar\omega, T) \left(\exp\left(\frac{\mu_i}{k_B T} \right) - 1 \right) d\omega \quad (7)$$

In heterogeneous systems, the total luminescence will be superposition of all emissive species i, which are defined by their respective absorption spectrum $A_i(\hbar\omega)$, radiative emission yield η_i, and applied chemical potential μ_i. For a typical OSC, at least three different emissive species – donor, acceptor, and interfacial CT states – can be identified. At first glance, Equation (7) does not distinguish between different types of applied potential, which would lead to equivalence of PL and EL emission fluxes ϕ_{PL} and ϕ_{EL}. In (experimental) reality, however, the excitation mechanisms are quite different. To go into more detail, we first focus on EL, as it is the reciprocal process to the extraction of photogenerated charge carriers, before discussing the differences to PL.

To induce EL, an electrochemical potential in form of an applied forward bias voltage $\mu_i = qV$ is applied to the contacts of an OSC, leading to an injection of free charge carriers, which, in the (in OPV dominant) case of CT recombination, recombine upon encountering the donor-acceptor interface. Equation (7) thus transforms into the electro-optical reciprocity relation given by Rau.[57] In the low injection regime, and due to a very low total EL quantum yield EQE_{EL} of OSCs, with typical reported values ranging from 10^{-8} to 10^{-4},[58,59] spectroscopic studies rely on quasi-steady state measurements with integration times greater than 1 ms. Since any transient effects will be negligible on this timescale and the free charge carriers from contacts being injected from thermal reservoirs, EL emission in the low-field regime in principle originates from non-geminate encounters between electrons and holes from populations that are in thermal equilibrium with the lattice.

In general, the spectral shape of the emission flux $\phi_{EL}(\hbar\omega)$ follows Equation (6), with a distinct line shape Γ centered around a maximum frequency ω_{EL}^{max}. For an exponentially disordered HOMO and LUMO, Gong et al. found that the EL maximum should exhibit a strong blueshift upon increasing μ_i of at least 30–60 meV per decade of injected current.[46] This behavior would be in contrast to Equation (7), where μ_i only increases the amplitude of ϕ_{EL}, yet has no influence on the respective spectral shape. Experimental evidence of such a shift was found by Deng et al., albeit at extremely high injected current densities above 1000 mA cm^{-2}.[60] Most experimental findings, including those by Gong et al., show consistently little or no such shift (see Figure 6).[15,18,46,48,61] In their work, Gong et al. further give a possible explanation of that discrepancy based on the comparably large distance between located sites in a disordered OSC leading to limited wave function overlap. The convolution of occupied donor HOMO and acceptor LUMO does not include that recombination of localized charge carriers may only occur between adjacent sites; as a consequence, radiative recombination requires at least one of the involved charge carriers being around the transport energy, that is, above its equilibrium energy.[46] Melianas et al. came to a similar conclusion by comparing measured EL spectra to kMC simulations for a Gaussian DOS.[18] While the charge carrier densities of injected free electrons and holes are in equilibrium with thermal reservoirs (the contacts) and the lattice at low fields, EL emission predominantly probes unrelaxed states within the DOS. Under the assumption that radiative recombination requires formation of a CT exciton first, the density of CT states should differ from the thermal population of the joint (convoluted) DOS of n and p; likewise, Burke et al. discussed an arbitrary, Gaussian density of CT states in thermal equilibrium with free charge carriers.[62]

Both Gong et al. and Tvingstedt et al. have found that while the integrated emission flux ϕ_{EL} depends on the applied potential, it is sensitive to parasitic effects like series resistances. These are likely to cause a deviation between applied μ_i and quasi-Fermi level splitting of free electrons and holes in the device.[46,63] By comparing JV and $\phi_{EL}(V)$, they were able to concur that the EL recombination yield is rather independent of the injected charge carrier density, with radiative ideality factors close to 1.[63] If the applied potential is large enough, μ_i can reach equilibrium with the density of donor or acceptor excitons as well, and induce emission from those species as well.[47,64,65] Since the radiative recombination from those singlets is usually much more efficient than from CT states ($\eta_{CT} < \eta_{A,D}$),[51,66] the total emission flux can in this case be dominated by single phase emission.[47,54,65] For higher applied potentials however, the OSC might be subject to both current-induced Joule heating,[48,67] leading to an increased lattice temperature, as well as non-equilibrium charge carrier densities.[60]

A similar effect can be observed in low driving force blends, when the energy barrier between CT states and acceptor singlets is comparably low, in the range of a few $k_B T$, or even absent. Here, thermal activation can lead to a significant occupation of the singlet species even at low applied potentials; with the larger $\eta_{A,D}$, ϕ_{EL} might be dominated by the singlet again.[51,66] In this case

**ADVANCED
SCIENCE NEWS**

www.advancedsciencenews.com

**ADVANCED
ELECTRONIC
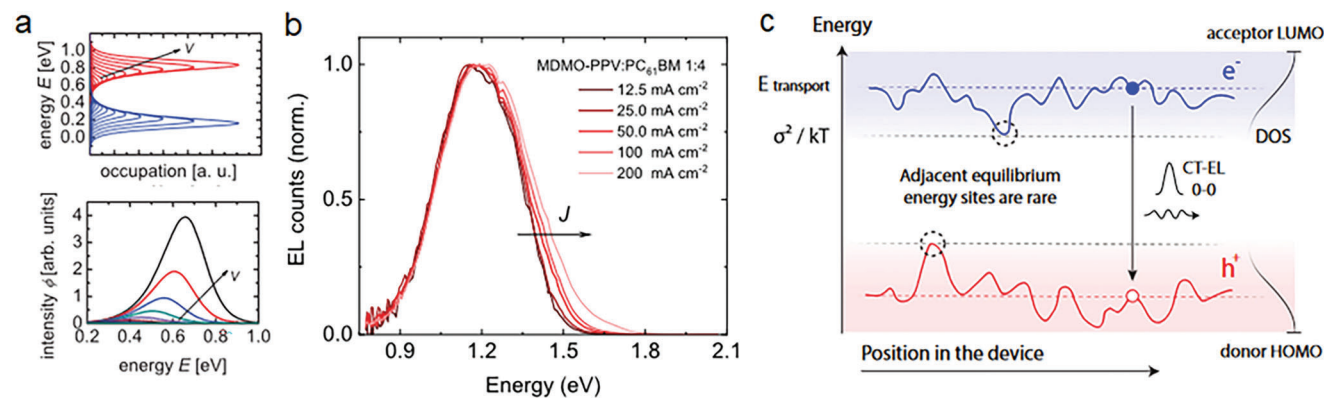MATERIALS**

www.advelectronicmat.de

Figure 6. a) Expected voltage-dependent EL peak shift of the convoluted occupied DOS from exponentially disordered HOMO and LUMO due to increased state filling by injected charge carriers.[46] b) Measured EL spectra with increasing injection current show little to no such shift. c) An explanation for spatially dispersed disordered sites in an OSC: recombination is only possible from charge carriers close to each other. Radiative recombination is therefore limited to a non-thermal subregion of the convoluted DOS from acceptor LUMO and donor HOMO. (a) Reproduced with permission.[46] Copyright 2012, The American Physical Society. (b) and (c) Reproduced with permission.[18] Copyright 2019, NAS.

and due to necessity of thermal activation, the spectral shape of $\phi_{EL}(\hbar\omega, T)$ shows a characteristic temperature dependence: the relative singlet intensity decreases at lower temperatures.[51]

This segue leads us to the often-discussed temperature dependency of ϕ_{EL}.[15,48,54,61,68] According to Equation (7), the shape of $\phi_{EL}(E, T)$ follows the grey body spectrum $A_i \cdot \phi_{BB}(\hbar\omega, T)$, which is equivalent to occupation by a Boltzmann statistic. For a Gaussian CT state DOS, the expected occupation should again be of Gaussian shape; its linewidth is given by convolution of the temperature-independent static disorder, temperature-dependent dynamic broadening (Figure 3), and $\phi_{BB}(\hbar\omega, T)$:[48,67] in general, the linewidth decreases at lower temperatures due to reduced dynamic broadening. Experimental evidence of this behavior was recently reported by Linderl et al., Khan et al., Göhler et al., and Tvingstedt et al. in small molecule donor:fullerene acceptor OSCs.[15,48,54,61] All studies agree on the qualitative behavior, yet reach different conclusions regarding the involvement of static and dynamic disorder based on their quantitative analyses. Incidentally, the latter three studies provided $\phi_{EL}(\hbar\omega, T)$ data for the same model system, a low donor content TAPC:C60 blend. A direct comparison of their spectra for three different temperatures and Gaussian linewidths at similar injection current densities is shown in Figure 7. Measured spectra differ significantly despite similar device architectures and measurement conditions; the reported extracted linewidths and their temperature gradients vary even more, with apparent saturation at low temperatures reported by Tvingstedt et al. Khan et al. concluded that the linewidth is dominated by the static disorder at low temperatures, and dynamic disorder only matters above a certain temperature,[61] while Tvingstedt et al. and Göhler et al. explained the behavior solely with dynamic disorder due to multiple high and mid energy vibrational modes.[15,48] The reported discrepancy in measured linewidths may reflect slight unintentional differences in the investigated OSCs; however, Göhler et al. also found that the empirical validity of Equation (7) in comparison with absorption measurements – used as a control for the emission temperature – deviates under low temperatures and increasing injection current densities, suggesting that the emission temperature can easily be underestimated in typical EL experiments. Additionally, they re-

ported that a dynamically broadened DOS is best able to explain radiative V_{OC} limits.[48] At least, these recent findings highlight that an analysis of temperature-dependent EL spectra alone is not necessarily reliable to reveal the static disorder of the CT DOS as suggested by Burke et al.[62]

The second discussion point refers to another main feature of EL emission. Most OSC EL studies show to some degree a temperature-dependent bathochromatic shift of ω_{EL}^{max}.[15,48,54,61] Linderl et al. and Göhler et al. suggested that static disorder should induce a shift $-\sigma_{DOS}^2/k_BT$ in thermal equilibrium, which would be much larger than any reported values in OSC. This analytical solution of Equation (7) is based, however, on the assumption that the DOS is infinitely broad, thus including a finite number of low-energy states to be filled at low temperatures. If, as the more realistic description of an OSC discussed by Gong et al. and Melianas et al. suggests, the emitting DOS is limited, this assumption will break down at low temperatures. In a follow-up based on an empirical suggestion by Yan et al.,[69] Göhler & Deibel introduced an analytical solution based on a Gaussian DOS artificially cut at a discretization minimum[68] – this would be equivalent to the spatially limited DOS of adjacent CT sites used by Melianas et al.[18] In this case, EL emission could occur from thermal equilibrium of injected charge carriers and emissive CT states at all temperatures without a significant bathochromatic shift.

A recent experiment by Lampande et al. provides strong evidence that the CT-EL lineshape is determined by dispersive, energy-dependent formation rates from (thermal) reservoirs of free electrons and holes.[70] The authors used modulation electroluminescence spectroscopy (MELS) to study the driving frequency dependence (magnitude and phase) of the electroluminescence intensity at different emission energies, see Figure 8 and the inset in panel (a). The experiments show a clear dispersion, with higher emission energies showing a faster response, which could quasi-quantitatively be explained by a simple model based on energy-dependent hopping rates, cf. panel (b). Interestingly, the same experiment showed non-dispersive recombination kinetics for a bilayer Alq3/NPB OLED, which the authors explain in terms of different correlations between the
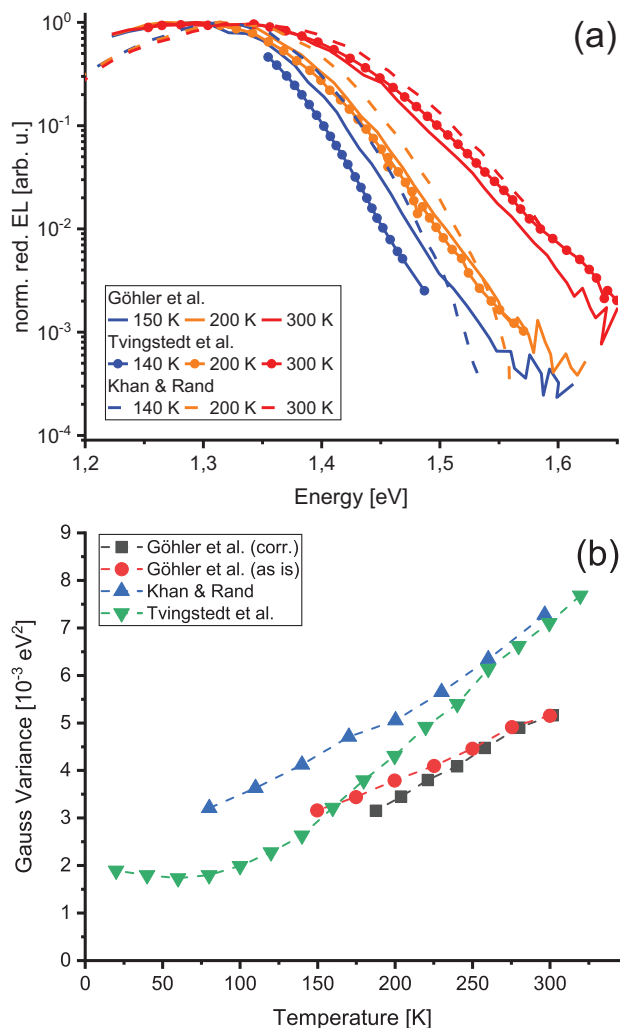
Figure 7. a) Reported reduced EL spectra from TAPC:C60 solar cells with 5–6.25% donor content in a 50 nm thick active layer. Since the device architecture and injection conditions (current density ≈150 mA cm⁻² for 3 exemplary temperatures) were reported as almost identical, the reason for the different emission spectra is not obvious. b) Reported Gaussian variances for the same system differ in quantity and temperature gradient. Göhler et al. utilized reciprocity with absorption measurements to correct for unintentional temperature deviations due to Joule heating, possibly explaining the differences in recorded spectra. (Data taken from [15,48,61]).

emission energy and the energies of the involved HOMO and LUMO energies for CT and direct exciton emission.[70] From the CT-EL results, the authors conclude "that the distribution of CT states formed by electrical injection in the dark is not in quasi-equilibrium", which seems to connect dispersive rates with the (im)possibility to have an equilibrium distribution. However, under the condition of detailed balance, the equilibrium distribution does not depend on the rates – e.g., charges hopping in a Gaussian DOS, with strongly energy-dependent rates, cf. Equation (3), still thermalizes to a Fermi-Dirac distribution. Still, the results are a direct confirmation of the assumptions that led Melianas et al. to argue that CT-EL originates from DOS site distributions significantly above DOS equilibrium energies.[18]

To summarize, EL studies have shown that emission from donor and acceptor singlets is quenched in OSCs in favor of CT emission,[47] which originates from a distinct emissive CT DOS that is populated from reservoirs of free charge carriers.[67] While the latter is, at low driving fields, in thermal equilibrium with the lattice, the emissive DOS cannot, in discrepancy to inorganic semiconductors, be identified with a simple convolution of HOMO and LUMO levels, filled with thermalized free charge carriers.[18,46] Instead, its filling rate is energy- and temperature-dependent and broadened by dynamic and static disorder.

An alternative to EL is available in PL, when emission is induced by photoexcitation, either with a broadband light source or a narrow-band laser. This enables PL to be excited selectively, by matching the incident photon wavelength distribution to the absorption A_i of the emissive species. Thus, the applied photochemical potential can be adjusted to either term i in Equation (7), e.g., by using a short wavelength laser absorbed only by high-energy donor states.[53] The individual photochemical potentials μ_i depend on the excitation conditions and absorption properties, as well as relaxation and transfer dynamics. In contrast, the applied electrochemical potential $\mu_i = qV$ for EL injection applies to every species. To avoid simultaneous EL emission and charge extraction, PL can be investigated under open-circuit conditions. Additionally, short laser pulses in combination with gated detectors or time-correlated photon counting modules enable transient techniques on much shorter time scales than the low quantum yield and capacitive time constants would allow for EL.[16,53,71]

Now, how does PL emission compare to EL in terms of probing the DOS in OSCs? Starting form transient PL experiments, it has been shown by Brigeman et al. that the initial CT PL emission of SubPC:C60 films are non-thermalized, thus relaxing to lower energies in the DOS within the first few ns; further, that steady state emission spectrum settles at higher average energies at lower temperatures (see Figure 9).[71] From these observations, they concluded that photoexcitation initially occupies states out of thermal equilibrium – independent of temperature under constant excitation – followed by a fast, yet incomplete, geminate recombination. Afterward, the free charge carrier densities thermalize much slower, with the final steady state determined by the thermally activated hopping processes in the disordered DOS, and recombination lifetime.

Kahle et al. used gated PL spectroscopy to investigate the behavior in OSCs with polymer donors, where they found the total ϕ_{PL} composed of two species: higher energy acceptor- and longer living CT PL, with the latter dominating the spectrum after several tens of ns.[16,53] From spectral deconvolution, they found a small geminate thermalization shift of the emission maxima ω_{PL}^{max}, and a similar blueshift of the steady-state spectrum at lower temperatures for systems with a large static disorder.[16] The unquenched PL of the acceptor species has been attributed to geminate excitons in unmixed acceptor phases which are unable to reach an interface for charge transfer. Felekidis et al. and Tvingstedt el al. highlighted that PL spectra should be corrected for this contribution to probe relevant emission from free charge carriers by taking the differential emission under open-circuit and short- (or reversed)-circuit conditions:[40,50,52]

$$\phi_{PL,CT}(\hbar\omega) \approx \phi_{PL}^{OC}(\hbar\omega) - \phi_{PL}(\hbar\omega, V \leq 0\ \text{V}) \tag{8}$$

**ADVANCED
SCIENCE NEWS**

www.advancedsciencenews.com

**ADVANCED
ELECTRONIC
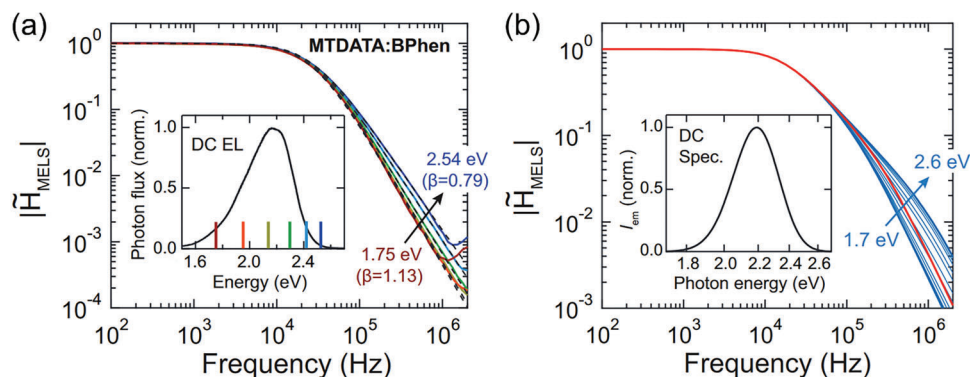MATERIALS**
Open Access

www.advelectronicmat.de

Figure 8. a) Experimental and b) calculated modulation electroluminescence spectroscopy (MELS) spectra for a 1:1 MTDATA:BPhen bulk heterojunction. a) The colored lines are the magnitude of the response for different emission energies from the CT-EL spectrum shown in the inset. The dashed black lines fit into a rate equation model. b) the same from a semi-analytical model based on an energy-dependent CT-formation rate τ_{rec}^{-1}. In absence of dispersion in τ_{rec}^{-1}, all recombination energies show the same frequency dependence (red line). Reproduced according to the terms of the CC BY license.[70] Copyright 2023, the authors, published by Wiley VCH.

Within $\phi_{PL}(V \leq 0 \text{ V})$ non-geminate CT emission will be quenched due to extraction of separated charge carriers. The open-circuit luminescence flux $\phi_{PL}^{OC}(\hbar\omega, T)$ is probably dominated by – potentially selectively induced – geminate PL, thus probing a different ensemble of states than EL. Consequently, Brigeman et al. and Kahle et al. both found the steady state EL spectrum bathochromatically shifted with respect to PL,[53,71] with other studies reporting a similar relation.[40,50,52,54] A somewhat trivial reason for this behavior could be the different excitation paths, with EL and PL probing different spatial regions of

the heterogeneous OSC. Similar effects have been reported for luminescence from mixed and planar heterojunctions of the same materials.[72] If the blend can be treated as well mixed, however, the discrepancy bolsters the assumption that EL is probing an already thermalized DOS, whereas PL is not.[53] However, both emission distributions can be almost identical in different systems with very low driving forces, like PM6:Y6.[50,51,73]

On that background, several studies discussed whether PL or EL is more suited to probe the relevant DOS for OSCs operation. Melianas et al. highlighted that luminescence emission might be
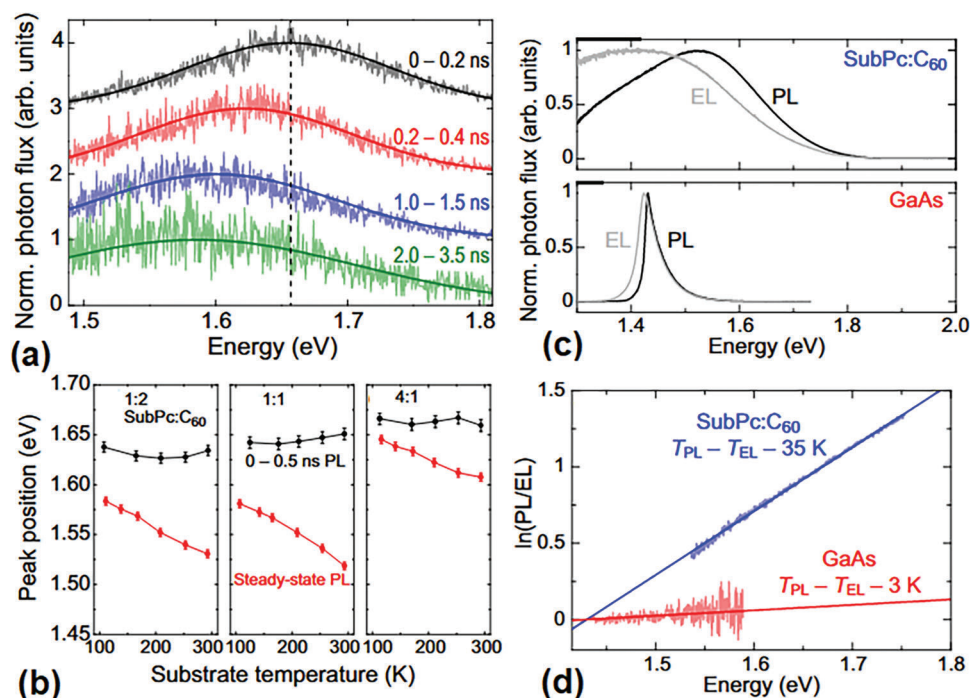

Figure 9. a) Evolution of measured PL emission of a SubPC:C60 solar cell at 300K in the first few ns shows energetic relaxation of the distribution. b) With decreasing temperature, the initial PL remains constant at high energies, while free charge carriers are unable to thermalize fully within their lifetime, leading to steady-state emission from higher average energy. c,d) A comparison between steady-state PL and EL emission at 300 K reveals a bathochromatic shift of $\phi_L(\hbar\omega)$ – equivalent to a higher temperature – if induced by an electric potential. The difference is more pronounced in disordered OSCs compared to an inorganic GaAs solar cell. Reproduced with permission.[71] Copyright 2018, APS.

**ADVANCED
SCIENCE NEWS**

www.advancedsciencenews.com

**ADVANCED
ELECTRONIC
MATERIALS**

www.advelectronicmat.de

limited to a subset of the total DOS,[18] leaving out non-emitting states. Khan & Rand argued that since these "hidden" states are potentially relevant for charge generation, recombination, and transport, but only reliably filled during EL injection, PL is less suitable.[61] Thus, drawing conclusions regarding electrical OSC properties, including open-circuit voltage, from PL emission is not trivial; this holds especially true for PL fluxes $\phi_{PL}^{OC}(\hbar\omega, T)$ under open-circuit conditions, which are potentially dominated by geminate recombination from excitons that do not produce free charge-carriers in the first place.

In their 2019 study, Kahle et al. discussed the temperature behavior of the PL emission of systems based on the donor polymer MeLPPP with regard to linewidth and position of the maxima ω_{PL}^{max}, as well as intensity transients. They argued that every aspect indicates a disordered DOS with non-thermalized PL emission. Due to the PL measurements being carried out under open-circuit conditions, the probed species might include geminate recombination as we discussed above; however, they also reported a more thermalized EL emission.[53] In a subsequent 2022 transient PL spectroscopy study, Kahle et al. argued that while photoexcited singlets do relax in the acceptor (donor) phase, subsequently formed CT excitons will remain stationary. As a consequence, PL emission from CT states is not fully thermalized with respect to the disordered CT DOS, and a peak shift, as proposed by Göhler et al. and Linderl et al.,[48,54] should not be observable. This would imply that the density of photogenerated CT excitons is not in thermal equilibrium with the total CT DOS.

Kahle et al. further implied that EL emission should behave the same way, based on the assumption that both generation pathway includes relaxed singlet states.[16] However, we would like to highlight that PL and EL generation cannot necessarily be treated equally, and especially in the case of short wavelength excitation where photogenerated singlet states carry significant excess energy compared to a CT exciton, regardless of the temperature. Singlet ensembles might thermalize depending on the temperature (as discussed above); however, the path toward CT formation should be less affected (Figure 2). If CT excitons are indeed energetically stationary, as was proposed by Kahle et al., the resulting CT PL emission is expected to be stationary as well. The mechanism is different for EL, where injected free charge carriers in equilibrium with the thermal reservoirs form CT states with respect to transport energy and accessibility of adjacent sites within the disordered DOS; as such, higher temperatures enable encounters in energetically higher states, resulting in an expected shift of the EL emission maximum with regard to temperature, only limited by a finite CT DOS.

In summary, while PL offers the upside of transient measurements to study thermalization effects,[53,71] a direct comparison to the relaxed emission from steady-state EL measurements is not trivial and has to be treated with caution.

2.2. Absorption-, Photocurrent- and Luminescent Spectra

The spectral dependence of the photocurrent is given by the external quantum efficiency (EQE$_{PV}$) spectrum, defined as the ratio between the flux of charges extracted at short circuit and the incident photon flux, as a function of photon energy (or wavelength). The shape of the EQE$_{PV}$ spectrum resembles the absorption spectrum ($A(\hbar\omega)$, Equation 2), i.e., the fraction of absorbed photons by the photo-active layer. When comparing EQE$_{PV}(\hbar\omega)$ and $A(\hbar\omega)$ spectra for organic photovoltaic devices, it is important that optical interference effects are taken into account.[22,23,74,75]

The EQE$_{PV}$ is related to A by the internal quantum efficiency (IQE):

$$EQE_{PV}(\hbar\omega) = A(\hbar\omega) \cdot IQE(\hbar\omega) \tag{9}$$

In the photon energy range where donor and/or acceptor absorbs strongly (above gap), often a constant IQE, not depending on the excitation energy, is measured,[22,23,74,75] while in some cases an IQE depending on whether donor or acceptor phase is excited is observed.[76,77] However for the highest-performance OPV devices IQE does not depend on photon energy for above-gap excitation and is between 90–100%.[10]

Reliable measurements of the IQE in the absorption tail region and below the optical gap of donor and acceptor, in the spectral region of CT absorption are very scarcely reported in the literature. Such measurements are difficult to perform, due to the weak absorption and strong photon energy dependence of $A(\hbar\omega)$ in that region, potentially resulting in large errors. Nevertheless, extending IQE measurements to the CT absorption region led to mixed results. On the one hand, no strong dependence on IQE was found at low photon energies for several polymer:fullerene devices, with the IQE staying within the same range as for above gap excitation.[13,78] On the other hand, a roll-off was found for both devices based on both fullerene and non-fullerene acceptors.[40,78–80]

Additional arguments for the absence of strong energy dependence of the IQE are based on experimental verifications of the reciprocity relation between absorption (or EQE$_{PV}$) and electroluminescence emission spectra $\phi_{EL}(\hbar\omega)$. The reciprocity relation allows to calculate the $A(\hbar\omega)$ spectrum from an emission spectrum under the condition that emission comes from a thermalized excited state population. This is based on the following reasoning:

In darkness and thermal equilibrium, the thermal emission spectrum $\phi_{th}(\hbar\omega)$ of the photo-active layer is given by Kirchoff's law of thermal radiation:

$$\phi_{th}(\hbar\omega) = A(\hbar\omega) \cdot \phi_{BB}(\hbar\omega) \tag{10}$$

Hereby is $\phi_{BB}(\hbar\omega)$ the black body spectrum at the temperature of the active layer. Under electrical or optical injection the total number of emitted photons ϕ_L drastically increases as compared to thermally emitted photons. However, in the case that the excited states thermalize before they emit, the spectral shape of the (non-thermal) emission spectrum for $E \gg k_B T$ will not change,[81] and therefore

$$\phi_L(\hbar\omega) \sim A(\hbar\omega) \cdot \phi_{BB}(\hbar\omega) \tag{11}$$

This relation can be used to determine $A(\hbar\omega)$ in the weakly absorbing spectra region, at photon energies where the emission spectrum can be accurately measured. When using electroluminescence spectra measured at low injection currents (to ensure conditions suitable for thermalization), one indeed often finds that the EQE$_{PV}(\hbar\omega)$ tail and the $A(\hbar\omega)$ spectrum calculated via
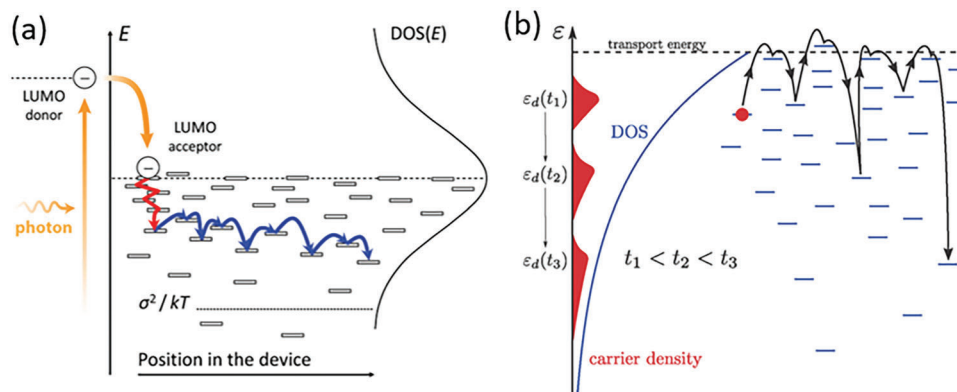
Figure 10. Schematic depictions of charge carrier thermalization in a medium with strong static disorder. a) At early times, excess energy is lost by fast, mostly diffusive motion (red arrow). At later times, the motion becomes more drift-dominated and is, therefore, more directed to the extracting electrode (blue arrows). Also in the latter process, the remaining excess energy is continuously lost, c.f. Figures 4 and 5. For disorder values typically encountered in OPV devices, charges are extracted from the device before reaching thermal equilibrium at σ^2/kT below the center of the DOS. Copyright 2019 Wiley. Used with permission from Melianas and Kemerink, Adv. Mater. 31, 1. (2019).[90] b) the same, for the later stages of thermalization. During thermalization, charges need to be excited from an intermediate trap site to the transport energy to be able to find deeper sites, which is not shown in (a), explaining the exponential slowdown of thermalization visible in Figure 4. Reproduced with permission.[33] Copyright 2014, Wiley VCH.

$\phi_L(\hbar\omega)/\phi_{BB}(\hbar\omega)$ coincide very well, implying a spectrally independent IQE in this spectral region.[51,80]

In several organic photovoltaic blends, however, electroluminescence and photoluminescence spectra differ from each other.[50,71] This implies that at least one of the two does not originate from an equilibrated excited state population.

2.3. Photocurrent

The steady-state short-circuit current density J_{sc} delivered by any kind of photovoltaic device can be determined via

$$J_{SC} = -e \int \phi_{ph}^{AM1.5}(\hbar\omega)\, EQE_{PV}(\hbar\omega)\, \hbar d\omega, \tag{12}$$

where $\phi_{ph}^{AM1.5}$ is the photon flux density of the AM1.5 solar spectrum. In practice, the short-circuit current can be reduced by a limited efficiency of the elementary processes in photocurrent generation (compare kinetic diagram). However, well-operating devices show internal quantum efficiencies close to unity,[82,83] so that $J_{SC} \approx J_{gen}$.

While in the discussion of steady-state photocurrents it is often implicitly assumed that there is unique material-dependent mobility, it has been shown experimentally by transient measurements that the extracted photocurrent is highly dispersive, meaning that either (i) the charge extraction times show a large spread over multiple orders of magnitude, (ii) the mobility strongly depends on time after photo-excitation,[84–91] (iii) the carrier concentration is time dependent[92] or (iv) a combination of these effects. The origin of the dispersive behavior, which is universally observed in both fullerene- and non-fullerene-based OPV devices, the question of whether charge carriers can be extracted before thermalization is complete and how this affects the steady-state behavior and the significance of measurement techniques is intensely debated.

Dispersion in extraction times occurs inherently because charge carriers are generated at different distances from the ex-

tracting electrode. However, the resulting linear broadening of the extraction time distribution alone is not sufficient to describe measured (supra-linear) distributions in OPV materials.[90] Instead, using time-resolved TREFISH and TPC measurements combined with kMC simulations, Melianas et al.[93] argue that in disordered semiconductors the thermalization of photogenerated carriers is, in contrast to inorganic semiconductors, relatively slow[34,87,90,93,94] and a two-step process (see Figure 10): at early time-scales (1-100 ns), a significant part of the excess energy, $1 - 2\sigma_{DOS}$, is lost by rapid diffusion as hops downwards in energy are predominant, as also expected on basis of the discussion of the Péclet number above.[84,89,95,96] At later time-scales, thermalization slows down as charges need to be excited to the transport energy ($\Delta E > 0$) to become mobile, which is a prerequisite for finding deeper sites, closer to the equilibrium energy.[33] The latter is highlighted by the upward arrows in panel (b) of Figure 10. Despite the slowdown, as time progresses, the population of photocreated charge carriers cools down further while charges move, by drift, toward the extracting electrodes.[89,90] Also on these longer time scales, diffusive motion remains important, leading to a significant probability that charges end up at the wrong contact.[97] As a consequence of these stochastic non-equilibrium processes, in disordered organic semiconductors, charge carriers generated at the same site in the active layer can be extracted at massively different times. When determining the extraction time distribution of photo-generated charges from measured pulse responses it was found that the extraction times span over orders of magnitude in time and at the mean extraction time ≈80% of the carriers are already extracted.[90,98]

Another consequence of the gradual thermalization of photogenerated charges in the disorder-broadened DOS would be that also the mobility of these charges would decrease with time after photoexcitation. When techniques with different time scales are combined so that the entire time range of pico-μs is covered, it becomes apparent, as shown in Figure 5, that mobility can have a significant time dependence and ultrafast time-resolved measurements can give higher mobility values than (near)

**ADVANCED
SCIENCE NEWS**

www.advancedsciencenews.com

**ADVANCED
ELECTRONIC
MATERIALS**

www.advelectronicmat.de

steady-state methods.[88,89,93,99] The time-dependence in mobility was confirmed by kMC simulations, while the simulated steady-state value predicted by simulations agreed well with the value determined by photo-CELIV.[88] A consequence of this is that steady-state techniques such as SCLC or photo-CELIV may significantly underestimate the mobility of photogenerated charges at operating conditions as the thermalization is considered to be slower than the carrier extraction, especially in thin devices with a large disorder σ_{DOS}.[93] At the same time, any the motion of charges that, at forward bias, are injected from a thermal reservoir, that is a contact, is likely to be governed by near-equilibrium mobility.

Conversely, many studies have shown that mobilities determined by SCLC can be applied in combination with drift-diffusion models to describe OPV devices,[100–103] and even transient signals can be well described by drift-diffusion simulations, however, only if mobility relaxation is accounted for the first 50 ns.[104] In this context Le Corre et al.[105–107] argued that under operating conditions, i.e., close to the maximum power point and at constant illumination such that the bottom of the DOS is filled, steady-state mobilities are suitable to describe the charge carrier transport. As reasoning, it is stated that in this case, the relaxation time should be much shorter[108] compared to experiments based on pulsed light on a device that is otherwise in the dark because in the latter case, the DOS is empty.

In contrast, Philippa et al.[92] argued that not a transient mobility but a time-dependent carrier concentration is responsible for the dispersion of the photocurrent, more precisely, the loss of carrier density to trap states during transport.

Jasiūnas et al.[109] aimed to combine the above-mentioned different (experimental) approaches, i.e., they consider both the dark case (empty DOS) as well as devices under continuous illumination (occupation of low energy states) at different working points (MPP and short-circuit). They show that in the ps-ns range, the mobility exhibits a strong time dependence, while concentration effects related to filling of low-energy states and whether high-efficient NFA devices are considered or not are less important. For the slower ns-µs range, the mobility behavior strongly depends on the system used. In this regime, NFA devices show only a weak dependence on mobility on state filling and field. In comparison, less efficient PCBM-based systems show that in the case of an "empty" DOS (i.e., in the dark or at high fields) trapping strongly influences the mobility, while filling the low energy states leads to a less time-dependent mobility. In summary, this shows that mobility is not a solid parameter to characterize transport in OPVs as it depends on the time scale and state filling.

It should be noted however that including the full morphology of BHJ films, incorporating the tortuosity of blend morphologies might also induce dispersion due to carriers getting "trapped" in so-called dead ends.[110]

2.4. Open Circuit Voltage – Thermodynamic Picture

The assumptions of a spectrally independent IQE and that the electroluminescence spectrum has the same spectral shape as the thermal emission spectrum, but with an increased total photon-flux determined by the Fermi-level splitting between electrons and holes, results in the following equation for the total integrated emitted photon flux ϕ_{EL}:[4,57]

$$\phi_{EL} = \int EQE_{PV}(\hbar\omega)\,\phi_{BB}(\hbar\omega)\left(\exp\left(\frac{\mu}{k_B T}\right) - 1\right)\hbar d\omega \tag{13}$$

where $\phi_{BB}(\hbar\omega)$ is the blackbody spectrum. Note also that Equation 13 is essentially the same as Equation 7, applied to a single mode of emission and integrated over energy. When perfectly selective contacts are used, all injected current is recombination current. The emitted photon flux thus originates from that fraction of the injected current J_{inj}, which results in radiative decay:

$$J_{inj} = \frac{q}{EQE_{EL}}\int EQE_{PV}(\hbar\omega)\,\phi_{BB}(\hbar\omega)\left(\exp\left(\frac{\mu}{k_B T}\right) - 1\right)\hbar d\omega \tag{14}$$

Hereby is the electroluminescence quantum efficiency EQE_{EL} the ratio between the total injected current and the current resulting in radiative decay, $EQE_{EL} = \frac{q\phi_{EL}}{J_{inj}}$

Evaluating the integral $e\int EQE_{PV}(\hbar\omega)\phi_{BB}\hbar d\omega$ as $J_{0,rad}$, we obtain the diode equation:

$$J_{inj} = J_0\left(\exp\left(\frac{\mu}{k_B T}\right) - 1\right) \tag{15}$$

With $J_0 = \frac{J_{0,rad}}{EQE_{EL}}$. EQE_{EL} can depend on the charge density, or injected current, for example, due to trap filling. In the case that the EL quantum efficiency depends on the injected charge carrier density, i.e., $EQE_{EL} \sim J_{inj}^{\alpha}$ with $\alpha > 0$ and at $\mu \gg k_B T$ the equation for the injected current becomes:[67]

$$J_{inj} \sim \exp\left(\frac{\mu}{n k_B T}\right) \tag{16}$$

With n representing the ideality factor, being equal to $n = \alpha + 1$.

At open-circuit, no net current is injected or extracted from the device and J_{inj} balances with the photocurrent J_{ph}. Voltage losses due to charge transport and series resistance are absent and in the case of perfectly selective contacts, the potential at open circuit, qV_{OC} equals the quasi-Fermi level splitting µ. In analogy to Equation 12, the photocurrent is given by

$$J_{ph} = q\int EQE_{PV}(\hbar\omega)\,\phi_{ph}^{AM1.5}(\hbar\omega)\,\hbar d\omega \tag{17}$$

Using $J_{inj} = J_{ph}$ and solving Equation 14 to $\mu = qV_{OC} \gg k_B T$ gives the following equation for V_{OC}:

$$V_{OC} = \frac{k_B T}{q}\ln\left(\frac{J_{ph}}{J_0}\right) \tag{18}$$

$$= \frac{k_B T}{q}\ln\left(\frac{\int EQE_{PV}(\hbar\omega)\,\phi_{ph}^{AM1.5}(\hbar\omega)\,d\omega}{EQE_{EL}^{-1}\int EQE_{PV}(\hbar\omega)\,\phi_{BB}(\hbar\omega)\,d\omega}\right)$$

This equation implies that the highest V_{OC} is obtained for those devices for which EQE_{EL} has the highest value. An upper limit for V_{OC} in the case of radiative recombination only

**ADVANCED
SCIENCE NEWS**

www.advancedsciencenews.com

**ADVANCED
ELECTRONIC
MATERIALS**

www.advelectronicmat.de

(EQE$_{EL}$ = 1) is given by the so-called radiative limit ($V_{OC,r}$):

$$V_{OC,r} = \frac{k_B T}{q} \ln\left(\frac{J_{ph}}{J_{0,r}}\right) \tag{19}$$

$$= \frac{k_B T}{q} \ln\left(\frac{\int EQE_{PV}(\hbar\omega)\, \phi_{ph}^{AM1.5}(\hbar\omega)\, d\omega}{\int EQE_{PV}(\hbar\omega)\, \phi_{BB}(\hbar\omega)\, d\omega}\right)$$

The measured open-circuit voltage is in that case, using Equation 18:

$$V_{OC} = V_{OC,r} - \frac{k_B T}{q} \ln\left(EQE_{EL}^{-1}\right) \tag{20}$$

This equation has been confirmed for several organic photovoltaic devices.[67,111–113] Progress in higher V_{OC} materials has indeed resulted in more luminescent OPV.[114–116]

The denominator of Equation 18 is determined by the low energy part of the EQE$_{PV}$ spectrum, since the blackbody spectrum at room temperature T is an exponentially decreasing function with photon energy. In the case that the tail of the EQE$_{PV}$ spectrum is dominated by CT state absorption with a CT state energy E_{CT} and reorganization energy λ, it can be described by a Gaussian[67]

$$EQE_{PV}(\hbar\omega) = \frac{f}{\hbar\omega\sqrt{4\pi\lambda k_B T}} \exp\left(-\frac{(\hbar\omega - E_{CT} - \lambda)^2}{4\lambda k_B T}\right) \tag{21}$$

Hereby indicates f the strength of the CT absorption band. Filling in into the denominator of Equation 18 gives an equation for V_{OC} of the form[67]

$$V_{OC} \approx E_{CT} - \frac{k_B T}{q}\ln\left(\frac{J_{ph} h^3 c^2}{q f 2\pi \left(E_{CT} - \lambda\right)}\right) - \frac{k_B T}{q}\ln\left(EQE_{EL}^{-1}\right) \tag{22}$$

With h being Planck's constant and c the speed of light. Note that under the assumption that the tail of the EQE$_{PV}$ spectrum can be described by a Gaussian of the form Equation 21, the extrapolation of V_{OC} to 0K will be equal to the extrapolation of E_{CT} to 0K. Furthermore, V_{OC} depends only very weakly on λ (under the assumption that EQE$_{EL}$ is not affected strongly by λ).

In the equilibrium picture, static Gaussian disorder can be added to the description of the CT band as:[62]

$$EQE_{PV}(\hbar\omega) \sim \exp\left(-\frac{(\hbar\omega - E_{CT} - \lambda)^2}{4\lambda k_B T + 2\sigma_{CT}^2}\right) \tag{23}$$

With σ_{CT} the standard deviation of the CT state density of states due to inhomogeneous broadening. The expression for the open-circuit voltage becomes of the form:

$$V_{OC} \approx E_{CT} - \frac{\sigma_{CT}^2}{2k_B T} - \frac{k_B T}{q}\ln(\ldots) \tag{24}$$

The experimentally observed deviation from a linear relation between V_{OC} and T at low T is therefore in some cases explained by inhomogenous broadening.[5,62] For very low temperatures, the assumption of a continuously broadened Gaussian DOS (Equation (23)) which is filled by a Boltzmann distribution
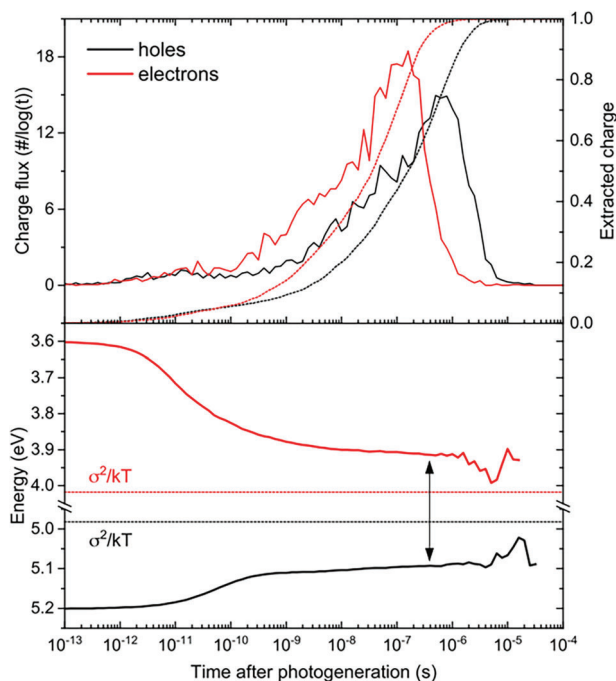

Figure 11. Energy loss after photoexcitation under open-circuit conditions for TQ1:PC$_{71}$BM. In the upper panel the extraction time distribution of photogenerated electrons (red solid line) and holes (black solid line) is shown, the corresponding integrated fraction of extracted charge is depicted as dotted lines. The lower panel shows the thermalization of photogenerated charges, i.e., the mean electron and hole energies (solid lines) in comparison to the equilibrium energies that lie $\sigma^2/k_B T$ below (above) the LUMO (HOMO) energy (dotted horizontal lines). Reprinted with permission.[97] Copyright 2021 American Chemical Society.

could break down, leading to higher $V_{OC,r}$ than expected from Equation (24).[68]

2.5. Open Circuit Voltage – Kinetic Picture

The concepts outlined above either explicitly or implicitly assume that photogenerated carriers are at the time of extraction in thermal equilibrium with the lattice. However, the outcomes of ultrafast charge extraction experiments, vide supra, and kMC simulations shown in Figure 11 demonstrate that this assumption may not be generic. When non-equilibrium effects are taken into account, the assumptions of the Shockley-Queisser limit would formally no longer apply to OPVs. Specifically, the assumption that all charge carrier populations are in thermal equilibrium with the lattice breaks down when thermalization is incomplete, as sketched in Figure 10. The pertinent question that then arises is whether non-equilibrium effects lead to any meaningful deviations from the near-equilibrium values of performance parameters that are predicted by a Shockley-Queisser-type analysis.

In general, there are two ways to examine whether the near-equilibrium limit can be exceeded with the help of non-thermalized charges:

(i) Models are used that take into account the slow relaxation of carriers in the disorder-broadened DOS, e.g. kMC simulations or multiple trapping and release models.[117] In contrast, the

**ADVANCED
SCIENCE NEWS**

www.advancedsciencenews.com

**ADVANCED
ELECTRONIC
MATERIALS**

www.advelectronicmat.de

drift-diffusion formalisms inherently assume that the carrier population is in thermal equilibrium with the lattice through the use of Boltzmann statistics. Upreti et al[97] demonstrate the consequences of this by simulating the relatively amorphous and disordered material system TQ1:PC$_{71}$BM: using an experimentally calibrated kMC model[98] and a drift-diffusion simulation with the same parameters. The authors then argue that any differences between the two models can be attributed to the drift-diffusion model failing to capture kinetic effects. The drift-diffusion model describes J_{SC} and the shape of the JV curve well, but underestimates V_{OC} by ≈ 0.2 V, while the kMC simulation correctly reproduces the full curve. Interestingly, this deviation in V_{OC} is largely independent of the device thickness and sample temperature. In contrast, systems that are less disordered show a smaller deviation in V_{OC} and in the limit that non-equilibrium effects are unimportant, drift-diffusion simulations accurately reproduce kMC calculations and experimental data.[97,118,119] In practice the above-described limitations of drift-diffusion simulations are often accounted for by increasing the (effective) band gap, which is however an artificial way to compensate for non-equilibrium effects. A major experimental challenge in this context is that, quite unlike the case for virtually all inorganic semiconductors, there is to date no experimental technique that allows to determine the position of the low energy part of the DOS that is relevant for charge transport.

(ii) In order to assess whether non-equilibrium effects indeed lead to higher PCEs than the thermodynamic non-equilibrium limit, determination of V_{OC} from the Shockley equation, which is based on charge carriers being in thermal equilibrium, as discussed in the preceding section, should be consistent with the outcomes of the kMC model in the vanishing disorder limit.

In the extended Shockley equation,

$$V_{OC} = \frac{k_B T}{q} \ln\left(\frac{J_{SC}}{J_0} + 1\right) + \frac{k_B T}{q} \ln\left(EQE_{EL}\right)$$
$$+ \frac{k_B T}{q} \ln\left(\frac{F_{coll}}{F_{inj}}\right) \tag{25}$$

The first term is the radiative limit for V_{OC} (compare Equation [19], while the second and third terms can, as detailed in Ref. [97,118] be determined from kMC simulations by looking at a device at $V = V_{OC}$ and in the dark. Dividing the integrated recombination current J_{EL} by the total injection current J_{inj} yields

$$EQE_{EL} = \frac{J_{EL}}{J_{inj}} \approx 0.14 \tag{26}$$

for TQ1:PC$_{71}$BM[97] and thus a reduction of V_{OC} compared to the equilibrium value of 0.05 V.

F_{coll} can be determined from the collection probability of photogenerated charges at position x in an active layer with thickness d via

$$F_{coll} = \frac{1}{d} \int_0^d f_c(x, V) \, dx = \frac{J_{ph}}{J_{gen}} \tag{27}$$

where J_{gen} is the maximum generated photocurrent that can be obtained from a transfer matrix model or via $J_{gen} = qG_{av}d$ with the average exciton generation rate G_{av}.

Moreover,

$$F_{inj} = \frac{1}{d} \int_0^d \frac{n(x, V)\, p(x, V) - n_i^2}{n_i^2 \left(\exp\left(qV/k_B T\right) - 1\right)} \, dx \tag{28}$$

where n and p are the electron and hole densities, and n_i the intrinsic charge density corresponding to the effective energy gap, $n_i^2 = N_0^2 \exp(-E_{gap}^{eff}/k_B T)$ with the site density $N_0 = a_{NN}^{-3}$. For the TQ1:PC$_{71}$BM system studied in Ref. [97] $F_{coll} \approx F_{inj}$ is found, leading to the third term being zero.

The reverse saturation current in the first term can be obtained from $q \int EQE_{PV}(\hbar\omega)\phi_{BB}(\hbar\omega)\hbar d\omega$ where the EQE_{PV} is given by Equation 9. Due to the steepness of the blackbody spectrum, only the energetically lowest parts of the CT and S_1 contributions to the absorption spectrum $A(\hbar\omega)$ are important and A can be written as:

$$A(\hbar\omega) = a\phi_{CT,Abs}(\hbar\omega) + b\phi_{S_1,Abs}(\hbar\omega) \tag{29}$$

where the CT and S_1 singlet absorption spectra can be calculated as convolutions of the relevant HOMO and LUMO levels, as discussed in Ref. [120] with their central energies corrected for the Coulomb binding energies of the S_1 and CT state. As organic semiconductors are strong absorbers, $b = 1$ is taken at the absorption maximum, while a can be determined from:

$$\frac{a}{b} = \frac{\nu_{CT}}{\nu_{S_1}} \frac{n_{s,CT}}{n_{s,S_1}} \tag{30}$$

where ν_{CT} and ν_{S_1} are the total CT and S_1 recombination rates used in the kMC model and n_s the number of absorption sites in the simulation box.

If the input parameters of the kMC model are used as described above to calculate the open circuit voltage from the Shockley equation, the corresponding equilibrium value is obtained, which is actually smaller than the V_{OC} obtained with the respective kMC simulation, but nearly equal to the value obtained by drift-diffusion.[97] Interestingly, the temperature dependence of V_{OC} was found to be nearly identical in kMC and drift-diffusion simulations.

Summarizing this section, V_{OC} is probably the performance characteristic of OPV where the differences between near- and far-from-equilibrium descriptions differ most, up to ≈ 0.2 V for moderately strong energetic disorder, which is massive. As both modeling approaches seem to get the experimental phenomenology right, there is a clear need to develop new experimental tests to distinguish the two. At the same time, any significant contributions of non-equilibrium effects to V_{OC} might open the way for new strategies to further enhance V_{OC}, as discussed in the Discussion and Outlook section below.

2.6. Recombination

Aspects of recombination have already been discussed above in the context of photo- and electroluminescence. Since these

ADVANCED
SCIENCE NEWS

www.advancedsciencenews.com
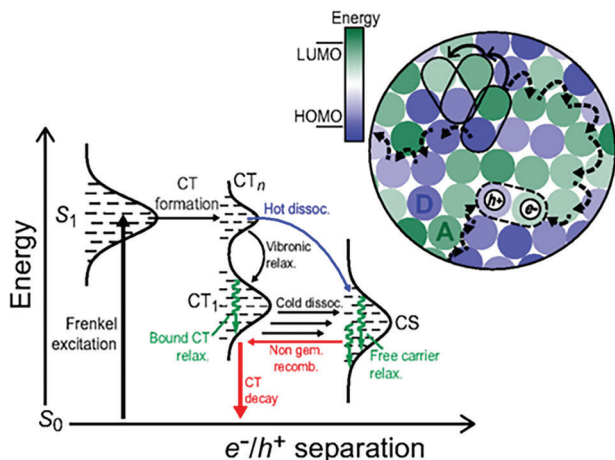
ADVANCED
ELECTRONIC
MATERIALS

www.advelectronicmat.de

Figure 12. Charge separation, relaxation, and recombination pathways within the disorder-broadened CT and free carrier density of states distributions in a typical OPV D-A blend. Once formed, CT states may relax geminately through correlated motion of the electron and hole toward lower-energy sites (Process 1, shown by the solid arrows in the inset) or they may dissociate into free carriers that relax independently and recombine to form nongeminate CT states (Process 2, shown by the dashed arrows). Reproduced with permission.[71] Copyright 2018, APS.

Figure 13. Schematic charge carrier kinetics in an OPV device at open circuit. Non-thermalized photocurrents (J_{photo}, green arrows) are balanced by thermalized injection currents (J_{inj}, blue arrows). Recombination (current J_{rec}, red arrows) is governed by "cold" charges injected from the contacts, while it is weak for "hot" photogenerated charges. Reproduced with permission .[128] Copyright 2021, American Chemical Society.

processes occur on ∼ns timescales that are long compared to the ∼ps timescales of on-site (vibronic) relaxation, the only way the recombination of photogenerated charges can be significantly affected through non-equilibrium effects is by incomplete thermalization in the DOS. Indeed, various authors have addressed this possibility, both experimentally[43,71,121,122] and theoretically/numerically.[43–45,62,123,124]

Clear optical signatures of recombination and thermalization of geminate electron-hole pairs occurring on similar, (sub-)ns, timescales have been observed in the form of transient red-shifts of photoluminescence spectra for singlet emission in neat materials,[125,126,43] for host-guest systems[126] and for CT emission in bulk heterojunctions.[71] For the singlet emission, a significant effect of the excitation energy was observed, with reducing or even inverting shifts for excitation deeper in the (disorder-broadened) S_1 manifold.[125,126] These results could quantitatively be explained by numerical simulations of incoherent hopping of excitations by a Förster-process in a Gaussian density of excited states.[43,125] Under typical conditions, the thermalization occurs on ns timescales and often does not saturate within the time range that can be experimentally resolved, indicating that thermalization of geminate pairs is a slow process that does not generally complete within the lifetime of the excitation.

Due to the generally strongly quenched luminescence in well-performing OPV systems, it is far from trivial to perform transient emission spectroscopy as would be needed to investigate the (non-) equilibrium nature of recombination in BHJ. Nevertheless, Brigeman et al. showed for the SubPc:C60 system that recombination leading to CT-PL stems from non-thermalized distributions.[71] Specifically, they distinguished between a thermalization process of geminate CT pairs that occurs on an ns-timescale, and a slower thermalization process of independent electron and hole populations that then can recombine nongeminately, as illustrated in Figure 12 and visible in the spectra
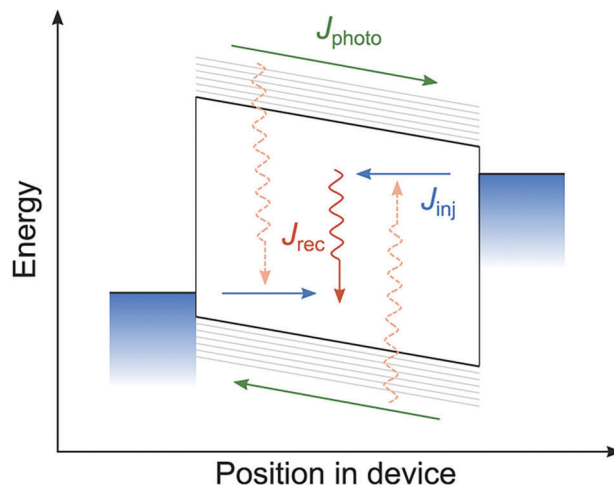
of Figure 9a. Neither of these processes was found to complete within the lifetime of the excitations, resulting in a CT state distribution that is thermal, but characterized by an effective temperature that exceeds that of the lattice. Although these results are, as argued by the authors, of generic nature, their quantitative impact on recombination strength or V_{OC} was not addressed.[71]

The results by Brigeman et al. are in part confirmed by those by Neher and coworkers, who used a time-delayed collection field (TDCF) to study the transient order and rate of recombination on time scales of tens of ns and beyond for a variety of polymer:PCBM BHJ OPV systems.[121,122,127] In these experiments, recombination at early times, up to several µs, was found to be strongly dispersive for more disordered systems (PCDTBT:PCBM, TQ1:PCBM), showing a pronounced slow-down of the recombination rate with time, which could be quasi-quantitatively understood in terms of thermalizing populations of photogenerated electrons and holes, c.f. process 2 in Figure 12.[121,122] On the other hand, more ordered systems (P3HT:PCBM) were found to exhibit nondispersive recombination over the full measurable time range.[127] For both strongly and less disordered systems, a steady-state bimolecular recombination rate k_2 was found, but not explained, that lies significantly below the (Langevin) value that is predicted on basis of equilibrium mobilities.[121,127] Interestingly, for the TQ1:PCBM system, it was found that energetic relaxation outpaces nongeminate recombination, leading to steady-state recombination that is dominated by equilibrated charges.[122] Although this led the authors to suggest that quasi-equilibrium concepts appear suited for describing V_{OC} in OPV despite significant energetic disorder, the observation of equilibrated charge carriers dominating the steady-state recombination can be reconciled with the kinetic, far-from-equilibrium picture proposed by Upreti et al. on basis of kinetic Monte Carlo simulations, see Figure 13[128] In this picture, even at V_{OC}, the vast majority of photogenerated charges avoid recombination and escape from the device on (sub--)µs timescales,

**ADVANCED
SCIENCE NEWS**

www.advancedsciencenews.com

**ADVANCED
ELECTRONIC
MATERIALS**

www.advelectronicmat.de

i.e., prior to full thermalization. The resulting net photocurrent is, at V_{OC}, compensated by an injection current coming from the contacts. As the contacts act as thermal reservoirs, this injection current consists of charges that are near equilibrium and recombine much stronger than the photogenerated ones.

The picture of charges thermalizing while recombining appears well-suited to address transient absorption spectroscopy. Indeed, TA spectra on PCDTBT:PCBM and TQ1:PCBM[36] (Figure 5a) covering a time range from ps to μs showed a clear transient red shift of the ground state bleach, which was attributed to hole thermalization in the polymer acceptor HOMO. Unfortunately, we are not aware of similar data for non-fullerene systems, which may be due to overlapping spectral features that make it hard if not impossible to single out weak redshifts.

From the experimental results discussed above, a consistent picture emerges that photogenerated charges in BHJ OPV are subject to a relatively slow thermalization in a disorder-broadened density of states. The recombination energy, rate, and order can be affected by ongoing thermalization, which is consistent with theoretical predictions. Apart from the already mentioned kMC simulations based on the Gaussian disorder model, the analytical model by Hofacker and Neher should be mentioned in this context.[124] The authors solve the transport energy model to show that recombination rates measured after pulsed excitation are inherently time-dependent, with apparent high-order recombination at short times. This notwithstanding, the question to which degree steady-state recombination in actual devices is affected by this "macroscopic hotness" is not yet unambiguously answered.

Turning to the absolute value of the uni- and bimolecular recombination rates of photogenerated charges, it has been recognized that kinetic effects, that is hopping rates that exceed the recombination rate of the bound pair, can cause a resplitting of an already formed CT or local exciton. This, in turn, provides the pair with (another) opportunity to escape recombination. Burke and McGehee argued that locally high equilibrium mobilities, for example, associated with easy transport along a conjugated chain, can explain experimentally observed high IQE values that would otherwise be inconsistent with a poorly screened Coulomb interaction.[129] In a later paper, the same authors argue that the resulting sub-Langevin value for the recombination rate actually implies an equilibrium between CT states and free charges.[62] Although their model accounts for energetic disorder in the form of a Gaussian-shaped distribution of CT states, it is based on the assumption of near thermodynamic equilibrium. The kinetic picture of CT states (re)splitting and (re)forming was independently proposed by Howard et al. on basis of numerical modeling by kMC of ultrafast transient spectroscopy data of PCDTBT:PCBM BHJ.[43] Here, the dynamic equilibrium between CT pairs and free charges results from the enhanced hopping rates of thermalizing charges and thus becomes a natural consequence of the presence of energetic disorder in typical OPV. By making the suppressed recombination an essentially transient effect that is associated with incomplete thermalization, the question arises to which degree the steady-state recombination is suppressed by it; this topic was not addressed in Ref. [43].

In a recent paper, Coropceanu et al. studied bimolecular recombination in BHJ using a kMC model that explicitly accounts for CT formation, splitting, and recombination.[44] Although a
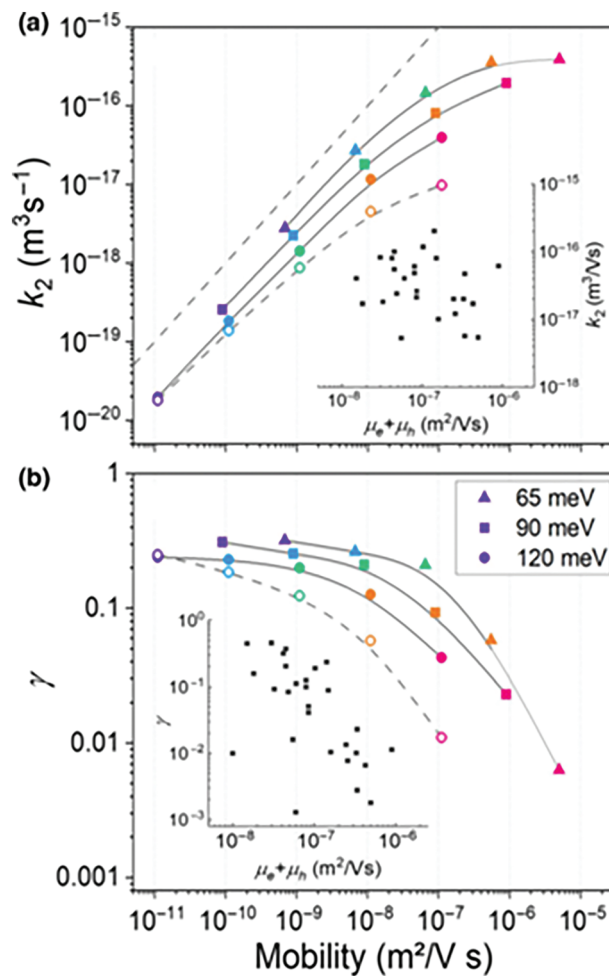

Figure 14. a) Simulated bimolecular recombination coefficient k_2 as a function of the mobility for energetic disorder of 65 (triangles), 90 (squares), and 120 meV (circles) for (nearly) equilibrated charges taken at different times. b) corresponding reduction factor. Solid symbols correspond to a recombination rate of $k_f = 10^8$ s^{-1}, while open circles show the results for $k_f = 10^7$ s^{-1} for $\sigma_{DOS} = 120$ meV. Dashed line is the prediction of the Langevin model; solid line guides the eye. The insets show experimental data for k_2 and γ as a function of $\mu_e + \mu_h$. Reproduced with permission.[45] Copyright 2021, American Physical Society.

direct connection to (equilibrium) mobility, and thereby to the Langevin value for recombination was not made in this work, it did show a strong decay in recombination rate with increasing disorder and CT lifetime. In addition, morphology was shown to be of significant importance in such a kinetic model for bimolecular recombination. In a later paper, Zuo et al. used a similar kMC model to investigate under which conditions said effects can lead to sub-Langevin recombination.[45] Depending on the ratio of the rate for dissociation k_d and the rate for recombination k_f, two regimes could be identified. In the encounter-dominated regime ($k_d \ll k_f$), recombination is proportional to mobility and only slightly reduced with respect to the Langevin limit, see panel (a) of Figure 14; in the resplitting-dominated regime ($k_d \gg k_f$), the bimolecular recombination rate k_2 is strongly suppressed and mobility is no longer the decisive parameter that determines k_2.

**ADVANCED
SCIENCE NEWS**

www.advancedsciencenews.com

**ADVANCED
ELECTRONIC
MATERIALS**

www.advelectronicmat.de

This leads to the counterintuitive finding that for a given mobility, larger energetic disorder (and concomitantly a larger hopping rate) is preferred, see Figure 14(b).[45]

A somewhat different approach to the themes discussed above was taken by Kaiser et al., who developed a model based on nonequilibrium thermodynamics to study charge separation in organic solar cells as a function of charge carrier delocalization and energetic disorder.[123] Somewhat in contrast to the kMC simulations discussed above, significant deviations from equilibrium are found for delocalized electron-hole pairs at small disorder; for high disorder, the free energy profile was found to be well-described as equilibrated.

2.7. Fill Factor

It is probably safe to say that the fill factor is one of, if not the least understood performance indicators of OPV devices. In the near-equilibrium Shockley model, Equation 15, the fill factor is not an independent parameter as it follows directly from the reverse saturation current J_0 and the temperature T, or equivalently from V_{OC} and T, and is independent of the short circuit or photocurrent. In more elaborate but still near-equilibrium models, the fill factor becomes a complex function of electron and hole mobilities, recombination and generation rates, active layer thickness, etc. On basis of extensive drift-diffusion calculations, Bartesaghi et al. have proposed a predictor α for the fill factor that is based on the ratio of the (equilibrium) rates for recombination and extraction of photogenerated charges.[102] Although a clear correlation with both measured and simulated fill factors was found, systems with α values that differ by more than an order of magnitude can still show the same fill factor, suggesting further work is needed.

We are not aware of any specific studies into the role of nonequilibrium effects on the fill factor, but the discussion of the Péclet number above suggests at least one scenario in which the enhanced diffusivity of non-thermalized charges enhances the probability that these diffuse against the (weak) extraction field and end up at the wrong contact. In case the contacts are not selective, the minority carrier will then recombine and be lost. As this effect becomes more pronounced for weaker extraction fields, it will lead to a reduced fill factor. Indeed, kinetic Monte Carlo simulations have suggested that this effect of interfacial recombination of "hot" minority carriers has a detrimental effect on the JV-curves of actual OPV devices.[97] The authors of Ref. [97] argue that in thinner devices, the incomplete saturation of the photocurrent at short circuits might be an indirect indication for this effect to actually occur. Further experiments, e.g. comparing devices with and without selective contacts, are needed to draw any final conclusions.

3. Discussion and Outlook

An important question that arises from the preceding discussions is whether any far-from-equilibrium effects can be exploited to "harvest" the excess energy of carriers that are not fully thermalized in the vibronic or electronic DOS and exceed the near-equilibrium thermodynamic limit of the same material. An OPV device operating on these concepts would be a truly "hot carrier" solar cell, where it has to be noted that in the community working on (inorganic) hot carrier solar cells, the hotness generally refers to an incomplete thermalization in a band, that is to vibronic hotness. In OPV and any other strongly disordered PV device, the transport directly after photogeneration and on-site thermalization, is, however, dominated by electronic hotness. As discussed in the context of Figures 10 and 11, this leads to a particularly large amount of energy getting lost through hopping to lower-lying sites, leading to a predominantly diffusive and thus stochastic motion. This diffusive transport can be rectified by introducing a vertical gradient in the donor:acceptor ratio, which breaks the symmetry that is needed for undirected diffusion by increasing the probability of holes (electrons) diffusing to the side of high donor (acceptor) content. This results in improved charge separation and extraction and subsequently in an increase in V_{OC} and FF, at least in numerical modelling.[130] Following up on that idea, it was shown that further tailoring the morphology to optimized phase-separated funnels leads indeed to a situation where the thermalization of photogenerated charges is slower than the carrier lifetime and a V_{OC} and PCE both surpassing the near-equilibrium limit.[118]

These funnel-shaped domains as introduced by Upreti et. al. reveal two key conditions to impose a maximal directional component to the initially diffusive motion and thereby achieve optimal, in silico, far-from-equilibrium OPV devices.[118] Throughout the entire active layer, the lateral feature size of the phase-separated funnels needs to be smaller than the diffusion length of the charge carriers for them to actually "feel" the asymmetry, and the narrow funnel ends need to be as narrow as possible. Using today's device fabrication methods, it seems impossible to realize these idealized morphologies in a top-down manner but it was speculated in Ref. 118] that both conditions can be fulfilled in state-of-the-art organic solar cells if vertical stratification is combined with spontaneous phase separation, leading to a bottom-up realization of vertical funnel-like features. This might for instance happen in films created with sequential deposition techniques or upon thermal annealing of composition gradients.[131–133] In Figure 15 we show the effects of improved phase-separation in kMC simulations before and after thermal annealing of active layers with a composition gradient. The thermal annealing procedure is based on the work by Peumans et al.[134] In short, different interaction energies are associated with homo (donor:donor and acceptor:acceptor) and hetero (donor:acceptor) interfaces. Minimizing the free (interfacial) energy by stochastically swapping sites then mimics the spontaneous phase-separation as expected upon thermally annealing a device. The functionality of this procedure becomes clear when starting with an entirely random 50:50 mixture of acceptor and donor states. As expected, thermal annealing then leads to a realistic representation of a bulk heterojunction, c.f. left column of Figure 15(b). More interesting, however, is the effect of spontaneous phase separation on a compositional gradient that begins with 90% acceptor and 10% donor states on one side of the device and varies linearly toward the opposite end. The feature size of each phase increases and funnel-like channels become visible, see the right column of Figure 15(b). The changes in morphology directly relate to improved device performance and FF as well as V_{OC} increases, see Figure 15(a). The direct comparison to the idealized 10–1 funnel structure that outperforms the

ADVANCED
SCIENCE NEWS

www.advancedsciencenews.com

ADVANCED
ELECTRONIC
MATERIALS
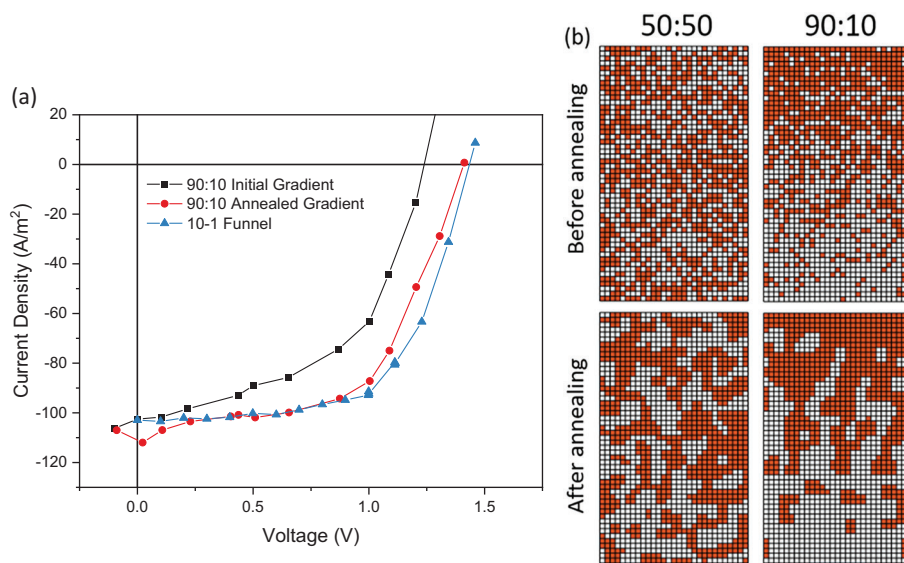
www.advelectronicmat.de

Figure 15. a) kMC simulations of vertical composition gradients before and after thermal annealing in comparison to an idealized funnel morphology. The initial donor (acceptor) concentration decreases linearly from 90% to 10% at the opposite end. The 10–1 funnel has a 10 × 10 unit cell and an inclusion of 1 × 1 site of acceptor material on one side which widens throughout the device until a 1 × 1 inclusion of donor is left on the opposite side of the device. All simulation parameters are chosen as defined by Upreti et al., i.e., the built-in potential of the simulated devices is 1 V.[118] b) Cross-sections of a random 50:50 donor:acceptor mix and a 90:10 composition gradient before and after thermal annealing.

near-equilibrium limit shows how much the gradient improves after thermal annealing. Applying the same analysis as used in Ref. [118] to analyze the funnels indeed reveals that the annealed gradient BHJ just outperforms the near-equilibrium limit.

Although composition gradients are not uncommon in OPV, we are not aware of any explicit experimental realizations of gradient devices exploiting non-equilibrium effects. This would make a worthwhile direction for further experimental and theoretical research that might shed light on some of the unsolved issues regarding the importance, or lack thereof, of nonequilibrium effects in OPV, while simultaneously leading to further device improvements. We note that even in near equilibrium, i.e., with charge carrier populations having the lattice temperature, concentration gradients provide an additional entropic potential difference across the device of[118,130]

$$V_{entr} = 2 \frac{k_B T_{eff}}{q} \ln\left(\frac{c_{D_0}}{1 - c_{D_0}} \right) \qquad (31)$$

where c_{D_0} and $1 - c_{D_0}$ are the relative fractions of donor material at the anode and cathode, respectively, and T_{eff} is the effective temperature of the charge carrier population that in that case would equal the lattice temperature.

The example of the gradient OPV, where non-equilibrium effects might contribute to V_{OC} and FF illustrates that the effects of static energetic disorder, in this case leading to slow thermalization, are not necessarily bad news. Nevertheless, it should be borne in mind that their driving force is ultimately energy loss. Likewise, the proposed enhancement in V_{OC} beyond its equilibrium value due to incomplete thermalization is still a "mitigation" of a loss process.[97] From a pragmatic device perspective, one should therefore probably focus primarily on materials

with reduced energetic disorder. Although often claimed otherwise, the so far limited measurements of energetic disorder of modern non-fullerene acceptor-based OPV do not suggest significantly lower values of σ_{DOS} than found in more old fashioned OPV systems, and reported numbers are by no means small, lying in the 60–90 meV range.[135–137] The latter means that, at least in the framework of the Gaussian disorder model, which is still the state-of-the-art for long-range charge transport in OPV materials, thermalization should be slow, as discussed in the theory section above. Any conclusive experimental proof of faster-than-expected thermalization would raise important questions regarding the underlying mechanism(s). A simple explanation in terms of filling of low-lying states, which would stop the thermalization at the quasi-Fermi level can be ruled out on basis of the low charge carrier densities in the bulk of typical OPV devices under operational conditions as discussed previously.[97]

Generalizing the above, it will be clear that strategies to further optimize OPV devices will, in many cases, strongly depend on whether or not state-of-the-art devices operate near or far from equilibrium. In the former case, mitigation of energy and recombination (fill factor) losses will likely continue along the lines that are currently being pursued: minimization of energy level offsets, reduction of non-radiative losses resp. enhancement of the luminescence quantum efficiencies, enhancement of mobilities in combination with reduction of energetic disorder, etc. Optimization by exploitation of non-equilibrium effects would, in contrast, require exploration of largely unknown territory. In view of the short on-site thermalization times, using vibronic hotness will likely be limited to the first few ps after charge generation and/or charge transfer. Here, one can imagine that materials with strongly delocalized wave functions can facilitate charge separation at a low driving force. As, even for small (<60 meV) disorder, global thermalization happens on much longer time scales, the

number of possible strategies to exploit this degree of hotness is probably larger. Nevertheless, the (re)use of thermalization energy will remain a partial mitigation of a loss channel: energetic disorder is bad, but not as bad as it could have been, and there might be ways to make it even less bad.

In summary, we have discussed the key (opto)electronic processes in energetically disordered organic solar cells, focusing on the connected questions to which degree these can be described by near-equilibrium concepts and models and how the performance indicators of current and future devices are affected. We have seen that models that rely on orthogonal assumptions regarding the importance of kinetics versus (near equilibrium) thermodynamics can give very satisfactory descriptions and even predictions of experimental observations. One reason for this appears to be the fact that, in many cases, there is a degree of freedom that allows to fit the data. An urgent example is the lack of experimental techniques to independently determine the position of the low-energy parts of the DOS that are relevant for charge transport. Having such a technique would allow truly quantitative predictions of V_{OC}.[18,40]

Conflict of Interest

The authors declare no conflict of interest.

[1] B. Ehrler, E. Alarcón-Lladó, S. W. Tabernig, T. Veeken, E. C. Garnett, A. Polman, *ACS Energy Lett.* **2020**, *5*, 3029.

[2] A. Köhler, H. Bässler, *Electronic processes in organic semiconductors: An introduction*.

[3] A. Armin, O. Li, O. J. Sandberg, Z. Xiao, L. Ding, J. Nelson, D. Neher, K. Vandewal, S. Shoaee, T. Wang, H. Ade, T. Heumüller, C. Brabec, P. Meredith, *Adv. Energy Mater.* **2021**, *11*, 2003570.

[4] K. Vandewal, K. Tvingstedt, A. Gadisa, O. Inganäs, J. V. Manca, *Nature Mater* **2009**, *8*, 904.

[5] J. C. Blakesley, D. Neher, *Phys. Rev. B* **2011**, *84*, 075210.

[6] J. Yuan, C. Zhang, B. Qiu, W. Liu, S. K. So, M. Mainville, M. Leclerc, S. Shoaee, D. Neher, Y. Zou, *Energy Environ. Sci.* **2022**, *15*, 2806.

[7] F. Laquai, D. Andrienko, C. Deibel, D. Neher, *In Elementary Processes in Organic Photovoltaics* (Ed.: K. Leo), Springer International Publishing, Cham, **2017**, 267.

[8] Q. Xie, X. Liao, L. Chen, M. Zhang, K. Gao, B. Huang, H. Xu, F. Liu, A. K.-Y. Jen, Y. Chen, *Nano Energy* **2019**, *61*, 228.

[9] S. M. Falke, C. A. Rozzi, D. Brida, M. Maiuri, M. Amato, E. Sommer, A. De Sio, A. Rubio, G. Cerullo, E. Molinari, C. Lienau, *Science* **2014**, *344*, 1001.

[10] Y. Lin, B. Adilbekova, Y. Firdaus, E. Yengel, H. Faber, M. Sajjad, X. Zheng, E. Yarali, A. Seitkhan, O. M. Bakr, A. El-Labban, U. Schwingenschlögl, V. Tung, I. McCulloch, F. Laquai, T. D. Anthopoulos, *Adv. Mater.* **2019**, *31*, 1902965.

[11] V. Gold, 4th Ed., *International Union of Pure and Applied Chemistry (IUPAC)*, Research Triangle Park, NC, **2019**.

[12] A. J. Gillett, A. Privitera, R. Dilmurat, A. Karki, D. Qian, A. Pershin, G. Londi, W. K. Myers, J. Lee, J. Yuan, S.-J. Ko, M. K. Riede, F. Gao, G. C. Bazan, A. Rao, T.-Q. Nguyen, D. Beljonne, R. H. Friend, *Nature* **2021**, *597*, 666.

[13] K. Vandewal, S. Albrecht, E. T. Hoke, K. R. Graham, J. Widmer, J. D. Douglas, M. Schubert, W. R. Mateker, J. T. Bloking, G. F. Burkhard, A. Sellinger, M. J. Fréchet, A. Amassian, M. K. Riede, M. D. McGehee, D. Neher, A. Salleo, *Nat. Mater.* **2014**, *13*, 63.

[14] A. E. Jailaubekov, A. P. Willard, J. R. Tritsch, W.-L. Chan, N. Sai, R. Gearba, L. G. Kaake, K. J. Williams, K. Leung, P. J. Rossky, X.-Y. Zhu, *Nature Mater* **2013**, *12*, 66.

[15] K. Tvingstedt, J. Benduhn, K. Vandewal, *Mater. Horiz.* **2020**, *7*, 1888.

[16] F. Kahle, A. Rudnick, S. Wedler, R. Saxena, R. Ammenhäuser, U. Scherf, S. Bagnich, H. Bässler, A. Köhler, *Adv. Energy Mater.* **2022**, *12*, 2103063.

[17] K. Vandewal, K. Tvingstedt, A. Gadisa, O. Inganäs, J. V. Manca, *Phys. Rev. B* **2010**, *81*, 125204.

[18] A. Melianas, N. Felekidis, Y. Puttisong, S. C. J. Meskers, O. Inganäs, W. M. Chen, M. Kemerink, *Proc. Natl. Acad. Sci. USA* **2019**, *116*, 23416.

[19] P. A. Lane, P. D. Cunningham, J. S. Melinger, O. Esenturk, E. J. Heilweil, *Nat. Commun.* **2015**, *6*, 7558.

[20] V. Abramavicius, V. Pranculis, A. Melianas, O. Inganäs, V. Gulbinas, D. Abramavicius, *Sci. Rep.* **2016**, *6*, 32914.

[21] G. Grancini, M. Maiuri, D. Fazzi, A. Petrozza, H.-J. Egelhaaf, D. Brida, G. Cerullo, G. Lanzani, *Nat. Mater.* **2012**, *12*, 29.

[22] M. Scharber, *Nature Mater* **2013**, *12*, 594.

[23] A. Armin, Y. Zhang, P. L. Burn, P. Meredith, A. Pivrikas, *Nature Mater* **2013**, *12*, 593.

[24] Y. Tamai, *Polym J* **2020**, *52*, 691.

[25] S. Gélinas, A. Rao, A. Kumar, S. L. Smith, A. W. Chin, J. Clark, T. S. van der Poll, G. C. Bazan, R. H. Friend, *Science* **2014**, *343*, 512.

[26] A. A. Bakulin, A. Rao, V. G. Pavelyev, P. H. M. van Loosdrecht, M. S. Pshenichnikov, D. Niedzialek, J. Cornil, D. Beljonne, R. H. Friend, *Science* **2012**, *335*, 1340.

[27] A. V. Nenashev, S. D. Baranovskii, M. Wiemer, F. Jansson, R. Österbacka, A. V. Dvurechenskii, F. Gebhard, *Phys. Rev. B* **2011**, *84*.

[28] D. Caruso, A. Troisi, *Proc. Natl. Acad. Sci. USA* **2012**, *109*, 13498.

[29] G. Zhang, X.-K. Chen, J. Xiao, P. C. Y. Chow, M. Ren, G. Kupgan, X. Jiao, C. C. S. Chan, X. Du, R. Xia, Z. Chen, J. Yuan, Y. Zhang, S. Zhang, Y. Liu, Y. Zou, H. Yan, K. S. Wong, V. Coropceanu, N. Li, C. J. Brabec, J.-L. Bredas, H.-L. Yip, Y. Cao, *Nat. Commun.* **2020**, *11*, 3943.

[30] S. Tscheuschner, H. Bässler, K. Huber, A. Köhler, *J. Phys. Chem. B* **2015**, *119*, 10359.

[31] D. Derewjanko, D. Scheunemann, E. Järsvall, A. I. Hofmann, C. Müller, M. Kemerink, *Adv. Funct. Mater.* **2022**, *13*, 2112262.

[32] J. Cottaar, L. J. A. Koster, R. Coehoorn, P. A. Bobbert, *Phys. Rev. Lett.* **2011**, *107*, 136601.

[33] S. D. Baranovskii, *Phys. Status Solidi B* **2014**, *251*, 487.

[34] H. Bässler, *Phys. Stat. Sol. (B)* **1993**, *175*, 15.

[35] L. Pautmeier, R. Richert, H. Bässler, *Philosophical Mag. Lett.* **1989**, *59*, 325.

[36] A. Melianas, F. Etzold, T. J. Savenije, F. Laquai, O. Inganäs, M. Kemerink, *Nat. Commun.* **2015**, *6*, 8778.

**ADVANCED
SCIENCE NEWS**

www.advancedsciencenews.com

**ADVANCED
ELECTRONIC
MATERIALS**
Open Access

www.advelectronicmat.de

[37] U. Albrecht, H. Bässler, *Chem. Phys. Lett.* **1995**, *235*, 389.

[38] H. van Eersel, R. A. J. Janssen, M. Kemerink, *Adv. Funct. Mater.* **2012**, *22*, 2700.

[39] A. Melianas, V. Pranculis, A. Devižis, V. Gulbinas, O. Inganäs, M. Kemerink, *Adv. Funct. Mater.* **2014**, *24*, 4507.

[40] N. Felekidis, A. Melianas, M. Kemerink, *J. Phys. Chem. Lett.* **2020**, *11*, 3563.

[41] C. Groves, N. C. Greenham, *Phys. Rev. B* **2008**, *78*, 155205.

[42] M. C. Heiber, C. Baumbach, V. Dyakonov, C. Deibel, *Phys. Rev. Lett.* **2015**, *114*, 136602.

[43] I. A. Howard, F. Etzold, F. Laquai, M. Kemerink, *Adv. Energy Mater.* **2014**, *4*, 1301743.

[44] V. Coropceanu, J.-L. Brédas, S. Mehraeen, *J. Phys. Chem. C* **2017**, *121*, 24954.

[45] G. Zuo, S. Shoaee, M. Kemerink, D. Neher, *Phys. Rev. Applied* **2021**, *16*, 034027.

[46] W. Gong, M. A. Faist, N. J. Ekins-Daukes, Z. Xu, D. D. C. Bradley, J. Nelson, T. Kirchartz, *Phys. Rev. B* **2012**, *86*, 024201.

[47] K. Tvingstedt, K. Vandewal, A. Gadisa, F. Zhang, J. Manca, O. Inganäs, *J. Am. Chem. Soc.* **2009**, *131*, 11819.

[48] C. Göhler, M. Saladina, Y. Wang, D. Spoltore, J. Benduhn, K. Leo, C. Deibel, *Phys. Rev. Applied* **2021**, *15*, 064009.

[49] J. Benduhn, K. Tvingstedt, F. Piersimoni, S. Ullbrich, Y. Fan, M. Tropiano, K. A. McGarry, O. Zeika, M. K. Riede, C. J. Douglas, S. Barlow, S. R. Marder, D. Neher, D. Spoltore, K. Vandewal, *Nat. Energy* **2017**, *2*, 17053.

[50] K. Tvingstedt, K. Vandewal, F. Zhang, O. Inganäs, *J. Phys. Chem. C* **2010**, *114*, 21824.

[51] L. Perdigón-Toro, L. Q. Phuong, S. Zeiske, K. Vandewal, A. Armin, S. Shoaee, D. Neher, *ACS Energy Lett.* **2021**, *6*, 557.

[52] K. Tvingstedt, J. Benduhn, K. Vandewal, *Mater. Horiz.* **2020**, *7*, 1888.

[53] F.-J. Kahle, A. Rudnick, H. Bässler, A. Köhler, *Mater. Horiz.* **2018**, *5*, 837.

[54] T. Linderl, T. Zechel, A. Hofmann, T. Sato, K. Shimizu, H. Ishii, W. Brütting, *Phys. Rev. Appl.* **2020**, *13*, 024061.

[55] M. Kasha, *Discuss. Faraday Soc.* **1950**, *9*, 14.

[56] P. Wurfel, *J. Phys. C: Solid State Phys.* **1982**, *15*, 3967.

[57] U. Rau, *Phys. Rev. B* **2007**, *76*, 085303.

[58] M. A. Green, A. W. Y. Ho-Baillie, *ACS Energy Lett.* **2019**, *4*, 1639.

[59] Y. Xie, W. Wang, W. Huang, F. Lin, T. Li, S. Liu, X. Zhan, Y. Liang, C. Gao, H. Wu, Y. Cao, *Energy Environ. Sci.* **2019**, *12*, 3556.

[60] W. Deng, W. Liu, R. Qian, H. Wu, *J. Phys. Chem. Lett.* **2022**, *13*, 544.

[61] S.-U.-Z. Khan, B. P. Rand, *Phys. Rev. Applied* **2021**, *16*, 044026.

[62] T. M. Burke, S. Sweetnam, K. Vandewal, M. D. McGehee, *Adv. Energy Mater.* **2015**, *5*, 1500123.

[63] K. Tvingstedt, C. Deibel, *Adv. Energy Mater.* **2016**, *6*, 1502230.

[64] U. Hörmann, J. Kraus, M. Gruber, C. Schuhmair, T. Linderl, S. Grob, S. Kapfinger, K. Klein, M. Stutzman, H. J. Krenner, W. Brütting, *Phys. Rev. B* **2013**, *88*, 235307.

[65] E. T. Hoke, K. Vandewal, J. A. Bartelt, W. R. Mateker, J. D. Douglas, R. Noriega, K. R. Graham, J. M. J. Fréchet, A. Salleo, M. D. McGehee, *Adv. Energy Mater.* **2013**, *3*, 220.

[66] T. Fritsch, J. Kurpiers, S. Roland, N. Tokmoldin, S. Shoaee, T. Ferron, B. A. Collins, S. Janietz, K. Vandewal, D. Neher, *Adv. Energy Mater.* **2022**, *12*, 2200641.

[67] K. Vandewal, K. Tvingstedt, A. Gadisa, O. Inganäs, J. V. Manca, *Phys. Rev. B* **2010**, *81*, 125204.

[68] C. Göhler, C. Deibel, *ACS Energy Lett.* **2022**, *7*, 2156.

[69] J. Yan, E. Rezasoltani, M. Azzouzi, F. Eisner, J. Nelson, *Nat. Commun.* **2021**, *12*, 3642.

[70] R. Lampande, A. Pizano, M. Gui, R. Cawthorn, B. P. Rand, N. C. Giebink, *Adv. Energy Mater.* **2023**, *13*, 2300394.

[71] A. N. Brigeman, M. A. Fusella, B. P. Rand, N. C. Giebink, *Phys. Rev. Appl.* **2018**, *10*, 034034.

[72] A. N. Bartynski, S. Grob, T. Linderl, M. Gruber, W. Brütting, M. E. Thompson, *J. Phys. Chem. C* **2016**, *120*, 19027.

[73] J. Yao, T. Kirchartz, M. S. Vezie, M. A. Faist, W. Gong, Z. He, H. Wu, J. Troughton, T. Watson, D. Bryant, J. Nelson, *Phys. Rev. Appl.* **2015**, *4*, 014020.

[74] G. F. Burkhard, E. T. Hoke, M. D. McGehee, *Adv. Mater.* **2010**, *22*, 3293.

[75] A. Armin, M. Velusamy, P. Wolfer, Y. Zhang, P. L. Burn, P. Meredith, A. Pivrikas, *ACS Photonics* **2014**, *1*, 173.

[76] S. D. Dimitrov, A. A. Bakulin, C. B. Nielsen, B. C. Schroeder, J. Du, H. Bronstein, I. McCulloch, R. H. Friend, J. R. Durrant, *J. Am. Chem. Soc.* **2012**, *134*, 18189.

[77] A. Armin, I. Kassal, P. E. Shaw, M. Hambsch, M. Stolterfoht, D. M. Lyons, J. Li, Z. Shi, P. L. Burn, P. Meredith, *J. Am. Chem. Soc.* **2014**, *136*, 11465.

[78] J. Lee, K. Vandewal, S. R. Yost, M. E. Bahlke, L. Goris, M. A. Baldo, J. V. Manca, T. V. Voorhis, *J. Am. Chem. Soc.* **2010**, *132*, 11878.

[79] M. Saladina, P. S. Marqués, A. Markina, S. Karuthedath, C. Wöpke, C. Göhler, Y. Chen, M. Allain, P. Blanchard, C. Cabanetos, D. Andrienko, F. Laquai, J. Gorenflot, C. Deibel, *Adv. Funct. Mater.* **2021**, *31*, 2007479.

[80] K. Vandewal, S. Albrecht, E. T. Hoke, K. R. Graham, J. Widmer, J. D. Douglas, M. Schubert, W. R. Mateker, J. T. Bloking, G. F. Burkhard, A. Sellinger, J. M. J. Fréchet, A. Amassian, M. K. Riede, M. D. McGehee, D. Neher, A. Salleo, *Nature Mater* **2014**, *13*, 63.

[81] P. Würfel, U. Würfel, *Physics of Solar Cells: From Basic Principles to Advanced Concepts*, John Wiley & Sons, Hoboken **2016**.

[82] Y. Lin, Y. Firdaus, M. I. Nugraha, F. Liu, S. Karuthedath, A. Emwas, W. Zhang, A. Seitkhan, M. Neophytou, H. Faber, E. Yengel, I. McCulloch, L. Tsetseris, F. Laquai, T. D. Anthopoulos, *Adv. Sci.* **2020**, *7*, 1903419.

[83] G. Zhang, X.-K. Chen, J. Xiao, P. C. Y. Chow, M. Ren, G. Kupgan, X. Jiao, C. C. S. Chan, X. Du, R. Xia, Z. Chen, J. Yuan, Y. Zhang, S. Zhang, Y. Liu, Y. Zou, H. Yan, K. S. Wong, V. Coropceanu, N. Li, C. J. Brabec, J.-L. Bredas, H.-L. Yip, Y. Cao, *Nat. Commun.* **2020**, *11*, 3943.

[84] I. A. Howard, F. Etzold, F. Laquai, M. Kemerink, *Adv. Energy Mater.* **2014**, *4*, 1301743.

[85] R. A. Street, K. W. Song, J. E. Northrup, S. Cowan, *Phys. Rev. B* **2011**, *83*, 165207.

[86] G. Schönherr, H. Bässler, M. Silver, *Philosophical Magazine B* **1981**, *44*, 47.

[87] R. Österbacka, A. Pivrikas, G. Juška, K. Genevičius, K. Arlauskas, H. Stubb, *Curr. Appl. Phys.* **2004**, *4*, 534.

[88] A. Melianas, V. Pranculis, A. Devižis, V. Gulbinas, O. Inganäs, M. Kemerink, *Adv. Funct. Mater.* **2014**, *24*, 4507.

[89] A. Melianas, F. Etzold, T. J. Savenije, F. Laquai, O. Inganäs, M. Kemerink, *Nat. Commun.* **2015**, *6*, 8778.

[90] A. Melianas, M. Kemerink, *Adv. Mater.* **2019**, *31*, 1806004.

[91] R. Jasiūnas, H. Zhang, J. Yuan, X. Zhou, D. Qian, Y. Zou, A. Devižis, J. Šulskus, F. Gao, V. Gulbinas, *J. Phys. Chem. C* **2020**, *124*, 21283.

[92] B. Philippa, M. Stolterfoht, P. L. Burn, G. Juška, P. Meredith, R. D. White, A. Pivrikas, *Sci. Rep.* **2014**, *4*, 5695.

[93] A. Melianas, V. Pranculis, Y. Xia, N. Felekidis, O. Inganäs, V. Gulbinas, M. Kemerink, *Adv. Energy Mater.* **2017**, *7*, 1602143.

[94] A. J. Mozer, G. Dennler, N. S. Sariciftci, M. Westerling, A. Pivrikas, R. Österbacka, G. Juška, *Phys. Rev. B* **2005**, *72*, 035217.

[95] D. A. Vithanage, A. Devižis, V. Abramavičius, Y. Infahsaeng, D. Abramavičius, R. C. I. MacKenzie, P. E. Keivanidis, A. Yartsev, D. Hertel, J. Nelson, V. Sundström, V. Gulbinas, *Nat. Commun.* **2013**, *4*, 2334.

[96] A. Devizis, K. Meerholz, D. Hertel, V. Gulbinas, *Phys. Rev. B* **2010**, *82*, 155204.

[97] T. Upreti, S. Wilken, H. Zhang, M. Kemerink, *J. Phys. Chem. Lett.* **2021**, *12*, 9874.

[98] S. Wilken, T. Upreti, A. Melianas, S. Dahlström, G. Persson, E. Olsson, R. Österbacka, M. Kemerink, *Sol. RRL* **2020**, *4*, 2001056.

[99] V. Gulbinas, *Lithuanian J. Phys.* **2020**, *60*, 1.

[100] V. D. Mihailetchi, H. X. Xie, B. de Boer, L. J. A. Koster, P. W. M. Blom, *Adv. Funct. Mater.* **2006**, *16*, 699.

[101] J. A. Bartelt, D. Lam, T. M. Burke, S. M. Sweetnam, M. D. McGehee, *Adv. Energy Mater.* **2015**, *5*, 1500577.

[102] D. Bartesaghi, I. del C Pérez, J. Kniepert, S. Roland, M. Turbiez, D. Neher, L. J. A. Koster, *Nat. Commun.* **2015**, *6*, 7083.

[103] C. M. Proctor, J. A. Love, T.-Q. Nguyen, *Adv. Mater.* **2014**, *26*, 5957.

[104] S. Albrecht, W. Schindler, J. Kurpiers, J. Kniepert, J. C. Blakesley, I. Dumsch, S. Allard, K. Fostiropoulos, U. Scherf, D. Neher, *J. Phys. Chem. Lett.* **2012**, *3*, 640.

[105] V. M. Le Corre, A. R. Chatri, N. Y. Doumon, L. J. A. Koster, *Adv. Energy Mater.* **2017**, *7*, 1803125.

[106] N. Felekidis, A. Melianas, L. E. Aguirre, M. Kemerink, *Adv. Energy Mater.* **2018**, *8*, 1800419.

[107] V. M. Le Corre, A. Rahimi Chatri, N. Y. Doumon, L. J. A. Koster, *Adv. Energy Mater.* **2018**, *8*, 1803125.

[108] N. J. Van Der Kaap, L. J. A. Koster, *Sci. Rep.* **2016**, *6*, 19794.

[109] R. Jasiūnas, V. Jašinskas, H. Zhang, T. Upreti, F. Gao, M. Kemerink, V. Gulbinas, *J. Phys. Chem. C* **2021**, *125*, 14567.

[110] M. C. Heiber, A. A. Herzing, L. J. Richter, D. M. Delongchamp, *J. Mater. Chem. C* **2020**, *8*, 15339.

[111] X.-K. Chen, D. Qian, Y. Wang, T. Kirchartz, W. Tress, H. Yao, J. Yuan, M. Hülsbeck, M. Zhang, Y. Zou, Y. Sun, Y. Li, J. Hou, O. Inganäs, V. Coropceanu, J.-L. Bredas, F. Gao, *Nat. Energy* **2021**, *6*, 799.

[112] S. M. Tuladhar, M. Azzouzi, F. Delval, J. Yao, A. A. Y. Guilbert, T. Kirchartz, N. F. Montcada, R. Dominguez, F. Langa, E. Palomares, J. Nelson, *ACS Energy Lett.* **2016**, *1*, 302.

[113] L. Zhang, R. Sun, Z. Zhang, J. Zhang, Q. Zhu, W. Ma, J. Min, Z. Wei, D. Deng, *Adv. Mater.* **2022**, *34*, 2207020.

[114] Q. Liu, S. Smeets, S. Mertens, Y. Xia, A. Valencia, J. D'Haen, W. Maes, K. Vandewal, *Joule* **2021**, *5*, 2365.

[115] P. Bi, S. Zhang, Z. Chen, Y. Xu, Y. Cui, T. Zhang, J. Ren, J. Qin, L. Hong, X. Hao, J. Hou, *Joule* **2021**, *5*, 2408.

[116] S. Ullbrich, J. Benduhn, X. Jia, V. C. Nikolis, K. Tvingstedt, F. Piersimoni, S. Roland, Y. Liu, J. Wu, A. Fischer, D. Neher, S. Reineke, D. Spoltore, K. Vandewal, *Nat. Mater.* **2019**, *18*, 459.

[117] N. Felekidis, A. Melianas, M. Kemerink, *Phys. Rev. B* **2016**, *94*, 035205.

[118] T. Upreti, C. Tormann, M. Kemerink, *J. Phys. Chem. Lett.* **2022**, *13*, 6514.

[119] W. F. Pasveer, J. Cottaar, C. Tanase, R. Coehoorn, P. A. Bobbert, P. W. M. Blom, D. M. de Leeuw, M. A. J. Michels, *Phys. Rev. Lett.* **2005**, *94*, 206601.

[120] N. Felekidis, A. Melianas, M. Kemerink, *J. Phys. Chem. Lett.* **2020**, *11*, 3563.

[121] J. Kurpiers, D. Neher, *Sci. Rep.* **2016**, *6*, 26832.

[122] S. Roland, J. Kniepert, J. A. Love, V. Negi, F. Liu, P. Bobbert, A. Melianas, M. Kemerink, A. Hofacker, D. Neher, *J. Phys. Chem. Lett.* **2019**, *10*, 1374.

[123] W. Kaiser, V. Janković, N. Vukmirović, A. Gagliardi, *J. Phys. Chem. Lett.* **2021**, *12*, 6389.

[124] A. Hofacker, D. Neher, *Phys. Rev. B* **2017**, *96*, 245204.

[125] S. C. J. Meskers, J. Hübner, M. Oestreich, H. Bässler, *J. Phys. Chem. B* **2001**, *105*, 9139.

[126] L. M. Herz, C. Silva, A. C. Grimsdale, K. Müllen, R. T. Phillips, *Phys. Rev. B* **2004**, *70*, 165207.

[127] J. Kniepert, I. Lange, N. J. van der Kaap, L. J. A. Koster, D. Neher, *Adv. Energy Mater.* **2014**, *4*, 1301401.

[128] T. Upreti, S. Wilken, H. Zhang, M. Kemerink, *J. Phys. Chem. Lett.* **2021**, *12*, 9874.

[129] T. M. Burke, M. D. McGehee, *Adv. Mater.* **2014**, *26*, 1923.

[130] O. Andersson, M. Kemerink, *Sol. RRL* **2020**, *4*, 2000400.

[131] H.-C. Wang, P. Cheng, S. Tan, C.-H. Chen, B. Chang, C.-S. Tsao, L.-Y. Chen, C.-A. Hsieh, Y.-C. Lin, H.-W. Cheng, Y. Yang, K.-H. Wei, *Adv. Energy Mater.* **2021**, *11*, 2003576.

[132] J. Qin, Q. Yang, J. Oh, S. Chen, G. O. Odunmbaku, N. A. N. Ouedraogo, C. Yang, K. Sun, S. Lu, *Adv. Sci.* **2022**, *9*, 2105347.

[133] M. Li, Q. Wang, J. Liu, Y. Geng, L. Ye, *Mater. Chem. Front.* **2021**, *5*, 4851.

[134] P. Peumans, S. Uchida, S. R. Forrest, *Nature* **2003**, *425*, 158.

[135] T. Upreti, Y. Wang, H. Zhang, D. Scheunemann, F. Gao, M. Kemerink, *Phys. Rev. Applied* **2019**, *12*, 064039.

[136] L. Perdigón-Toro, L. Q. Phuong, F. Eller, G. Freychet, E. Saglamkaya, J. I. Khan, Q. Wei, S. Zeiske, D. Kroh, S. Wedler, A. Köhler, A. Armin, F. Laquai, E. M. Herzig, Y. Zou, S. Shoaee, D. Neher, *Adv. Energy Mater.* **2022**, *12*, 2103422.

[137] R. Shi, H. Hu, T. Chen, R. Gui, J. Liu, X. Hao, H. Yin, *ChemPhysMater* **2023**, *2*, 52.

Dorothea Scheunemann obtained a Ph.D. in physics from the University of Oldenburg in 2016. After postdoctoral fellowships at Åbo Akademi (Finland), Linköping University, and Chalmers (Sweden), she has been a postdoc in Martijn Kemerink's group at the Institute for Molecular Systems Engineering and Advanced Materials (IMSEAM) at Heidelberg University since 2021. Her current research focuses on the physics of organic semiconductors and devices for energy harvesting.

Clemens Göhler studied Physics at the Technische Universität Chemnitz, where he received his Ph.D. in experimental physics on electro-optical excitation and emission spectroscopy of organic donor:acceptor solar cells. Since 2022 he has moved to a Post-Doc position in Prof. Kemerink's group at Heidelberg University. His research topics cover charge-transfer state characteristics and charge extraction losses of organic solar cells in the steady state.

Constantin Tormann is a Ph.D. candidate at the Institute for Molecular Systems Engineering and Advanced Materials (IMSEAM), Heidelberg University. His current research interests include charge and energy transport in disordered materials with a focus on the interplay of non-equilibrium effects and morphology in organic photovoltaics.

Koen Vandewal obtained his PhD in Physics at Hasselt University in 2009 working on the physics of organic photovoltaics. After that, he spent two years as a Postdoctoral Fellow at Linköping University in Sweden and another two years at Stanford University (USA). In 2014, he was appointed as an endowed professor at the Technische Universität (TU) Dresden in Germany. In January 2018, he moved from TU Dresden to Hasselt University, leading a research group with the aim to solve fundamental questions in the field of organic, hybrid, and molecular electronics with relevance to applications in electronic devices.

Martijn Kemerink obtained a Ph.D. in applied physics from Eindhoven University of Technology in 1998. Since 2019, he is a professor in Hybrid and Organic Devices at the Institute for Molecular Systems Engineering and Advanced Materials (IMSEAM) at Heidelberg University. His research interests include charge and energy transport in disordered materials, organic photovoltaics and thermoelectrics, organic ferro- and piezoelectrics, and ratchets.

2300293 (23 of 23)